Part I

Grid Synchronization Instability of Inverter Based Resources

Saeed Lotfifard
Hassan Yazdani, Graduate Student

Washington State University

For information about this project, contact

Saeed Lotfifard
Washington State University
School of Electrical Engineering and Computer Science
Pullman, Washington 99164-2752
Phone: 509-335-0903
Email: s.lotfifard@wsu.edu

Power Systems Engineering Research Center

The Power Systems Engineering Research Center (PSERC) is a multi-university Center conducting research on challenges facing the electric power industry and educating the next generation of power engineers. More information about PSERC can be found at the Center's website: http://www.pserc.wisc.edu.

For additional information, contact:

Power Systems Engineering Research Center
Arizona State University
527 Engineering Research Center
Tempe, Arizona 85287-5706
Phone: 480-965-1643
Fax: 480-727-2052

Notice Concerning Copyright Material

Table of Contents

1. Grid synchronization instability of inverter based resources 1
   1.1 Background 1
   1.2 Modeling of transfer function of inverters controllers 1
      1.2.1 Brief review of the structure of controllers 2
      1.2.2 Transfer function without the PLL 5
      1.2.3 Effects of the PLL dynamics 6
      1.2.4 The transfer function model with PLL dynamics 9
   1.3 Impedance-based stability analysis 12
   1.4 The Nyquist criterion: SISO to MIMO 14
   1.5 Analysis of impacts of different parameters on the stability of the inverters 15
      1.5.1 Results without considering the PLL dynamics 17
      1.5.2 Impedance/admittance with the PLL dynamics 18
      1.5.3 Stability analysis using the GNC plots. 20
   1.6 Case study results of impacts of line outages on grid synchronization stability of inverters 25
   1.7 Supplementary controller for enhancing inverters grid synchronization stability 27
   1.8 Conclusions 31

References 32

List of Figures

Figure 1.1 Schematic of a generic grid connected inverter 2
Figure 1.2 Current (inner) controller of the inverter 5
Figure 1.3 Block diagram of the transfer function of the system without considering PLL 6
Figure 1.4 dq synchronous reference frames of the system and the controller 7
Figure 1.5 Schematic of synchronous reference frame PLL 7
Figure 1.6 Block diagram of the transfer function of system with PLL dynamics 11
Figure 1.7 Schematic of the impedance based modeling of the grid connected VSC 13
Figure 1.8 Schematic of the interconnection of the grid and VSC equivalents 13
Figure 1.9 Generic model of SISO feedback system 143
Figure 1.10 s-plane contour of the right half plane 154
Figure 1.11 Representation of impedance stability analysis as a closed loop system 135
Figure 1.12 Schematic of a 2×2 MIMO system 16
Figure 1.13 Different combinations of VSC and grid equivalent models 16
Figure 1.14 Zdd impedance of the VSC in the absence of PLL dynamics 17
Figure 1.15 Ydd admittance of the VSC in the absence of PLL dynamics 18
Figure 1.16 dq channel impedance of the VSC 19
Figure 1.17 dq channel admittance of the VSC 19
Figure 1.18 qq channel impedance of the VSC 20
Figure 1.19 qq channel admittance of the VSC 20
Figure 1.20 GNC plots for $Rg = 0.08\ \Omega$ and $Lg = 8 \times 10 - 4$ H 21
Figure 1.21 GNC plots for $Rg = 0.09\ \Omega$ and $Lg = 9 \times 10 - 4$ H 22
Figure 1.22 GNC plots for $Rg = 0.12\ \Omega$ and $Lg = 1.2 \times 10 - 3$ H. 22
Figure 1.23 GNC plots ignoring the off-diagonals for $Rg = 0.08\ \Omega$ and $Lg = 8 \times 10 - 4$ H.... 23
Figure 1.24 Complete and unstable case with $Rg = 0.092\ \Omega$ and $Lg = 9.2 \times 10 - 4$ H and $kpPLL = 4.46$ and $kiPLL = 991$ 24
Figure 1.25 Simplified cased with $Rg = 0.092\ \Omega$ and $Lg = 9.2 \times 10 - 4$ H and $kpPLL = 4.46$ and $kiPLL = 991$, wrongly reported as stable. 24
Figure 1.26 GNC for a weak grid while ignoring the PLL dynamics 25
Figure 1.27 Schematic of the simulated multi-machine power system including an IBR 26
Figure 1.28 Output power of IBR, showing loss of grid synchronization subsequent to the sudden change in the strength of the system 266

Figure 1.29 Output power of IBR, showing IBR retain its synchronization with the grid by making slowing the PLL dynamic response. 27
Figure 1.30 Schematic 27
Figure 1.31 Schematic of the supplementary controller 288
Figure 1.32 Schematic 29
Figure 1.33 Schematic 31

List of Tables

Table 1 Parameters of the VSC [3] 17

NOMENCLATURE

Acronym

CPA	Cauchy's principle of argument
GNC	Generalized Nyquist criterion
IBR	Inverter-based resource
MIMO	Multi-input multi-output
PI	Proportional integral
PLL	Phase-locked loop
POI	Point of injection
PWM	Pulse width modulation
SCR	Short circuit ratio
SG	Synchronous generator
SISO	Single-input single-output
SRF	Synchronous reference frame
SS	Small signal
VSC	Voltage source converter

Parameters

v_{dc}	DC-side voltage of the VSC
R_f	Resistance of the VSC filter
L_f	Inductance of the VSC filter
Z_f	Matrix representation of the VSC filter
R_g	Resistance of the grid
L_g	Inductance of the grid
Z_g	Matrix representation of the grid impedance
ω_0	Synchronous speed
k_p, k_i	Current controller PI coefficients
k_p^{PLL}, k_i^{PLL}	PLL PI coefficients

i_{dq}^{ref}	Current references in the dq frame
Z_{vsc}	Output impedance of the VSC
Y_{vsc}	Output admittance of the VSC
$V_{i,dq}^{c}, V_{i,dq}^{s}$	Steady state input voltage of the VSC in the controller and system dq frames, respectively
$V_{o,dq}^{c}, V_{o,dq}^{s}$	Steady state output voltage of the VSC in the controller and system dq frames, respectively
I_{dq}^{c}, I_{dq}^{s}	Steady state output current of the VSC in the controller and system dq frames, respectively
V_{vsc}, I_{vsc}	Thevenin and Norton source equivalents of the VSC, respectively
Z_{line}	Impedance of the transmission line
Y_{load}	Admittance of the load
Z_{SG}	Impedance of the synchronous generator

Operators

$\mathbf{G}_{ci}$	Matrix representation of the PI controller
$\mathbf{G}_{dei}$	Decoupling matrix
$\mathbf{T}_{dq}$	dq frame transformation matrix
$\mathbf{T}_{\Delta\theta}$	System to controller dq transformation matrix
$\mathbf{T}_{PLL}$	Transfer function of the PLL
$\mathbf{T}_{vi}$	Voltage to current transformation of PLL dynamics
$\mathbf{T}_{vv}$	Voltage to voltage transformation of PLL dynamics
$\overline{\boldsymbol{\sigma}}(.), \underline{\boldsymbol{\sigma}}(.)$	Maximum and minimum singular values, respectively
$d(s)$	Characteristic function of the generic control system
$m(s)$	Transfer function of the generic control system
$g(s), h(s)$	Gain and feedback of the SISO generic control system
$\mathbf{G}(s), \mathbf{H}(s)$	Gain and feedback of the MIMO generic control system

Variables

$v_{i,abc}^{s}$	Input voltage of the VSC in the abc frame
$v_{o,abc}^{s}$	Output voltage of the VSC in the abc frame
i_{abc}	Output current of the VSC in the abc frame

v_g	Thevenin equivalent of the grid's voltage
x_{abc}	Sample signal in the abc frame
θ	Angle in the dq frame
i_{dq0}	Output current of the VSC in the abc frame
$v_{o,dq0}$	Output voltage of the VSC in the abc frame
$v_{i,dq0}$	Input voltage of the VSC in the abc frame
$\Delta\theta$	Angle difference between the controller and the grid dq frames
$\Delta v_{i,dq}^{c}, \Delta v_{i,dq}^{s}$	Small signal perturbation of input voltage of the VSC in the controller and system dq frames, respectively
$\Delta v_{o,dq}^{c}, \Delta v_{o,dq}^{s}$	Small signal perturbation of output voltage of the VSC in the controller and system dq frames, respectively
$\Delta I_{dq}^{c}, \Delta I_{dq}^{s}$	Small signal perturbation of output current of the VSC in the controller and system dq frames, respectively
u, y	Input and output of the generic control system
λ_1, λ_2	Eigenvalues of the MIMO characteristic loop gain

1. Grid synchronization instability of inverter based resources

1.1 Background

With the proliferation of renewable resources, the number of grid integrated inverter-based resources increases. Studying the grid synchronization stability of IBRs is critical. In this project impacts of different parameters such as PLL bandwidth and strength of the system are studies. Especially, IBRs dominated power grids may face significant reduction in the grid strength. Some situations that may lead to weak power grids at IBRs sites are as follows[1]:

- Installation of IBRs at remote wind/solar rich areas far from generation/load centers which are connected to the rest of the power grid through long distance lines. Examples of such sites are west Texas area wind farms [2] and several Australian power plants such as Musselroe and Silverton wind power plants [3] and Kennedy energy-park [4]. For instance, in the case of Kennedy energy-park in Australia in normal condition SCR is about 1.5 and during N-1 contingency SCR is about 0.7.
- Installation of IBRs at sites that despite being located at the vicinity of the generation/load center areas, they are not well integrated into the main power grid. For instance, Tehachapi wind site in California is located near the load center but connected to the main grid by a weak 66 kV system [5].
- Sudden reduction of the power system strength subsequent to outages of lines as the result of a fault occurrence in the power grid. For instance, First Solar PV power plant in Arizona experienced a significant reduction in the system strength due to line outages [6]. According to the report case study results, at SCR of 4 the damping was insufficient and the PV power plant was tripped.
- Installation of IBRs at islanded power system such as a Mediterranean island that is studies in [7]. Also, system splits that may occur due to cascading outages or controlled islanding could lead to islands with reduced system strength at IBRs sites [8].

In this project to systematically show the impacts of different parameters on grid synchronization stability of IBRs, bode plots and Generalized Nyquist Criterion (GNC) based on impedance-based stability analysis are utilized. To this end, the transfer functions of grid connected inverter is derived. The model includes the dynamic response of PLL which will be used by GNC and bode plots to show the impacts of different parameters on the grid synchronization stability of inverters. Then, to enhance the grid synchronization stability of inverter, a supplementary controller is implemented that adds damping to the main controllers of IBRs to damp out the oscillations on the output powers of IBRs subsequent to the occurrences of outages in the power system.

1.2 Modeling of transfer function of inverters controllers

In this section first a brief review of the structure of inverters controllers is presented. Then the procedure for deriving transfer functions of inverters is explained. The derived transfer functions will be used to study the impacts of different factors on the synchronization stability of inverters such as the parameters of synchronization mechanism of inverters and strength of the host power grid.

1.2.1 Brief review of the structure of controllers

In this section the structure of controllers of inverters is briefly explained which will be used in later sections for study the response of inverters to the disturbances. More detailed explanations of the inverter controllers can be found in [9]. Figure 1.1 shows a typical grid connected three-phase inverter. Based on its control logic, a IBRs can be operated either as a grid following source using a PLL, or as a grid forming source that mimics the behavior of legacy synchronous generators. In this report we consider the former. As depicted in Figure 1.1, the grid model is represented as Thevenin equivalent, which is a three-phase source, series with a resistor and an inductor.

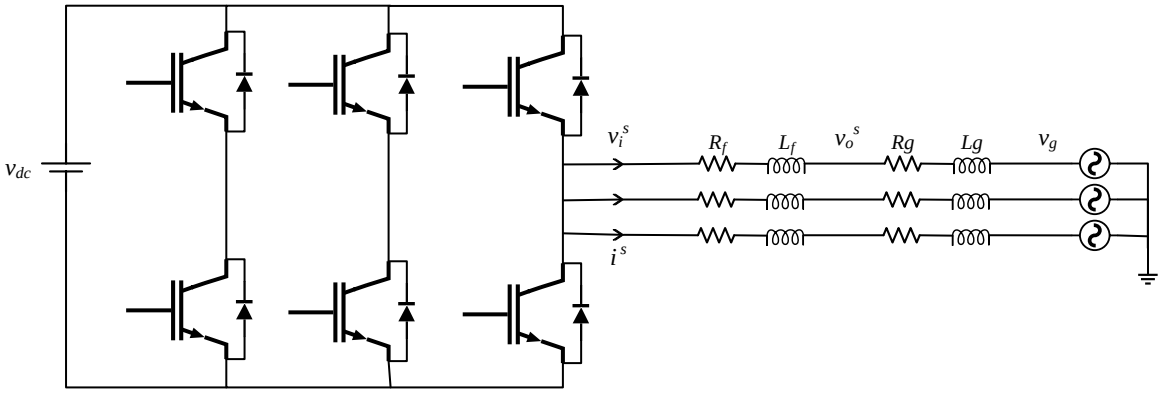

Figure 1.1 Schematic of a generic grid connected inverter

To begin with, the equations in the abc frame, between the input voltage and the output voltage of the inverter is written as (1.1) where v_{ia}, v_{ib}, and v_{ic} denote the input voltage of the inverter on each phase and similarly, v_{oa}, v_{ob}, and v_{oc} are the output voltages, and i_a, i_b, and i_c are the output currents. Also, R_f and L_f are the resistance and the inductance of the series filter. For simplicity, since the signals are all in the same reference frame, superscript s is not shown in the following equations.:

$$\begin{bmatrix} v_{ia} \\ v_{ib} \\ v_{ic} \end{bmatrix} - \begin{bmatrix} v_{oa} \\ v_{ob} \\ v_{oc} \end{bmatrix} = R_f \begin{bmatrix} i_a \\ i_b \\ i_c \end{bmatrix} + L_f \frac{d}{dt} \begin{bmatrix} i_a \\ i_b \\ i_c \end{bmatrix} \tag{1.1}$$

To simplify the analysis of the equations in (1.1), the park transformation (also known as dq transformation) is used. This transformation was first introduced in the early 1920s as a mathematical tool to facilitate the analysis of rotating electrical machines, in particular, the SGs, and offers numerous advantages. For instance, in the abc frame, the relationship between the phases is trigonometric, whereas in the dq frame there are two axes related in a linear fashion. Moreover, by using the dq frame, the control frame is aligned with the rotor frame with the synchronous frequency, allowing the utilization of synchronous reference frame control which is much more intuitive. In addition, in the dq frame control of the inverter, the design allows the independent control of active power and reactive power, which is extremely beneficial in managing the output of the inverter, facilitating its voltage and frequency alignment with the grid's reference frame. Using the Park transformation matrix, any three-phase signal x in the abc frame can be transformed to the $dq0$ frame, as depicted in (1.2):

$$\begin{bmatrix} x_d \\ x_q \\ x_0 \end{bmatrix} = \underbrace{\frac{2}{3}\begin{bmatrix} \cos(\theta) & \cos(\theta - \frac{2\pi}{3}) & \cos(\theta + \frac{2\pi}{3}) \\ -\sin(\theta) & -\sin(\theta - \frac{2\pi}{3}) & -\sin(\theta + \frac{2\pi}{3}) \\ \frac{1}{\sqrt{2}} & \frac{1}{\sqrt{2}} & \frac{1}{\sqrt{2}} \end{bmatrix}}_{\mathbf{T}_{dq}} \begin{bmatrix} x_a \\ x_b \\ x_c \end{bmatrix} \tag{1.2}$$

The inverse of $\mathbf{T}_{dq}$ is represented in (1.3) and by definition, $\mathbf{T}_{dq} \times \mathbf{T}_{dq}^{-1} = I_{3\times 3}$.

$$\mathbf{T}_{dq}^{-1} = \begin{bmatrix} \cos(\theta) & -\sin(\theta) & 1 \\ \cos\left(\theta - \frac{2\pi}{3}\right) & \sin\left(\theta - \frac{2\pi}{3}\right) & 1 \\ \cos\left(\theta + \frac{2\pi}{3}\right) & \sin\left(\theta + \frac{2\pi}{3}\right) & 1 \end{bmatrix} \tag{1.3}$$

By applying this transformation to (1.1), (1.4) is derived as follows:

$$\mathbf{T}_{dq}^{-1} \times \left(\begin{bmatrix} v_{ia} \\ v_{ib} \\ v_{ic} \end{bmatrix} - \begin{bmatrix} v_{oa} \\ v_{ob} \\ v_{oc} \end{bmatrix} \right) = R_f \mathbf{T}_{dq}^{-1} \times \begin{bmatrix} i_a \\ i_b \\ i_c \end{bmatrix} + L_f \frac{d}{dt} \left(\mathbf{T}_{dq}^{-1} \times \begin{bmatrix} i_a \\ i_b \\ i_c \end{bmatrix} \right) \tag{1.4}$$

The derivative of the second term on the right-hand side of (1.4) can be further simplified using the chain rule, as stated in (1.5):

$$L_f \frac{d}{dt} \left(\mathbf{T}_{dq}^{-1} \times \begin{bmatrix} i_a \\ i_b \\ i_c \end{bmatrix} \right) = L_f \left(\frac{d}{dt} \mathbf{T}_{dq}^{-1} \right) \begin{bmatrix} i_a \\ i_b \\ i_c \end{bmatrix} + L_f \mathbf{T}_{dq}^{-1} \times \frac{d}{dt} \left(\begin{bmatrix} i_a \\ i_b \\ i_c \end{bmatrix} \right) \tag{1.5}$$

To further simplify (1.5), first the derivative of the Park transformation is calculated as shown in (1.6)

$$\frac{d}{dt} \mathbf{T}_{dq}^{-1} = \begin{bmatrix} 0 & \frac{d}{dt}\theta & 0 \\ -\frac{d}{dt}\theta & 0 & 0 \\ 0 & 0 & 0 \end{bmatrix} \mathbf{T}_{dq}^{-1} \tag{1.6}$$

Then, by assuming the dq frame rotates with the synchronous speed, it results $\theta = \omega_s t$. By multiply $\mathbf{T}_{dq}$ to equation (1.4), (1.7) is derived. In (1.7), v_{id}, v_{iq}, and v_{i0} are the $dq0$ axes signals of the input voltage and similarly, v_{od}, v_{oq}, and v_{o0} are the output voltages in the $dq0$ frame. Also, i_d, i_q, and i_0 are the output currents in the $dq0$ frame.

$$\begin{bmatrix} v_{id} \\ v_{iq} \\ v_{i0} \end{bmatrix} - \begin{bmatrix} v_{od} \\ v_{oq} \\ v_{o0} \end{bmatrix} = R_f \begin{bmatrix} i_d \\ i_q \\ i_0 \end{bmatrix} + L_f \frac{d}{dt} \begin{bmatrix} i_d \\ i_q \\ i_0 \end{bmatrix} + L_f \frac{d}{dt} \begin{bmatrix} \omega_s i_q \\ -\omega_s i_d \\ 0 \end{bmatrix} \tag{1.7}$$

By rearranging the right-hand side, and since the 0 axis is equal to zero, (1.8) is derived in which s is the Laplace operator.

$$\begin{bmatrix} v_{id} \\ v_{iq} \end{bmatrix} - \begin{bmatrix} v_{od} \\ v_{oq} \end{bmatrix} = \begin{bmatrix} sL_f + R_f & -\omega_0 L_f \\ \omega_0 L_f & sL_f + R_f \end{bmatrix} \begin{bmatrix} i_d \\ i_q \end{bmatrix} \tag{1.8}$$

This can also be written as the two axis current equations, as written in (1.9) and (1.10). The d-axis current in (1.10) represents a signal that is in-phase with the inverter's output voltage, through which the active power output of the inverter can be controlled. On the other hand, the q-axis current is 90 degrees out of phase with the inverter's output voltage, through which the reactive power output of the inverter is controlled.

$$\frac{di_d}{dt} = \frac{1}{L_f}(v_{id} - R_f i_d + \omega_0 L_f i_q - V_{od}) \tag{1.9}$$

$$\frac{di_q}{dt} = \frac{1}{L_f}(v_{iq} - R_f i_d - \omega_0 L_f i_d - V_{oq}) \tag{1.10}$$

The inverter is equipped with a current controller, also known as the inner loop controller, as depicted in Figure 1.2. The objective of this controller is to set the inverter to output a specified amount of current, i_d^{ref} and i_q^{ref}, which can be achieved by manipulating the output voltage of the inverter through an PWM switching scheme. For simplicity, the PWM switching delays are considered negligible (fast) enough to be ignored.

This current controller is implemented according to the following stages. First, the reference values for the controller to track are generated. In most practical cases, an outer loop is also implemented, and the current reference values are generated through that higher level controller. Otherwise, these references should be calculated separately for the inverter to meet a specific criterion. Next, output current of the inverter is measured to generate the error value. Once these errors are generated, using a PI controller, a control action and an integral action accompanied by the coupling terms generate input voltage values for the VSC, such that the desired reference tracking of the dq frame current is achieved. Finally, in a closed loop fashion, these voltage values are utilized to adjust the switching patterns of the inverter, such that the control objective is satisfied dynamically.

Based on Figure 1.2, the equations for the inverter's voltage on each axis is written as (1.11) and (1.12), respectively. These voltage equations are the fundamental characteristic of the inverter and could be utilized to tune the current controller bandwidth through manipulating the PI controller coefficients.

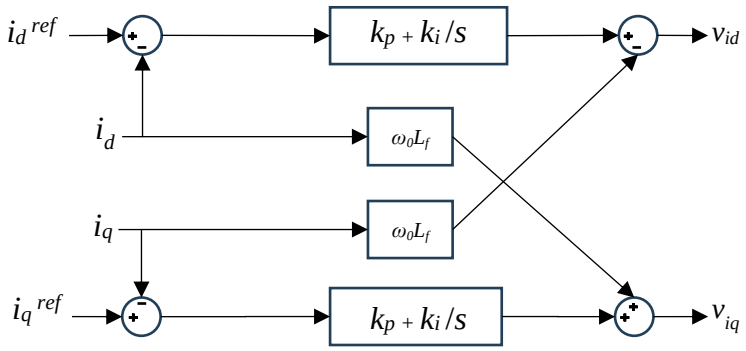

Figure 1.2 Current (inner) controller of the inverter

$$v_{id} = -\omega_0 L_f i_q + k_p\left(i_d^{ref} - i_d\right) + k_i\int (i_d^{ref} - i_d)dt \tag{1.11}$$

$$v_{iq} = \omega_0 L_f i_d + k_p\left(i_q^{ref} - i_q\right) + k_i\int (i_q^{ref} - i_q)dt \tag{1.12}$$

1.2.2 Transfer function without the PLL

In this section and next section, the transfer functions of inverters are derived. In deriving the transfer function procedures presented in [10-11] will be followed. However, compared to them the transfer functions derived in this project are more suitable for grid integration studies as transfer functions are derived such that they do not become too complex by ignoring fast dynamic components such as PWM and measurement filters. Equations (1.11) and (1.12) are rewritten as (1.13) where $\mathbf{G}_{ci}$ and $\mathbf{G}_{dei}$ are the current controller and decoupling matrices, respectively.

$$\begin{bmatrix} v_{id} \\ v_{iq} \end{bmatrix} = \underbrace{\begin{bmatrix} k_p + \dfrac{k_i}{s} & 0 \\ 0 & k_p + \dfrac{k_i}{s} \end{bmatrix}}_{\mathbf{G}_{ci}} \begin{bmatrix} i_d^{ref} \\ i_q^{ref} \end{bmatrix} - \left(\begin{bmatrix} k_p + \dfrac{k_i}{s} & 0 \\ 0 & k_p + \dfrac{k_i}{s} \end{bmatrix} + \underbrace{\begin{bmatrix} 0 & \omega_0 L_f \\ -\omega_0 L_f & 0 \end{bmatrix}}_{\mathbf{G}_{dei}} \right) \begin{bmatrix} i_d \\ i_q \end{bmatrix} \tag{1.13}$$

Using this representation, the block diagram of the system is formed, as shown in Figure 1.3 where Z_f is the matrix representation of the VSC filter.

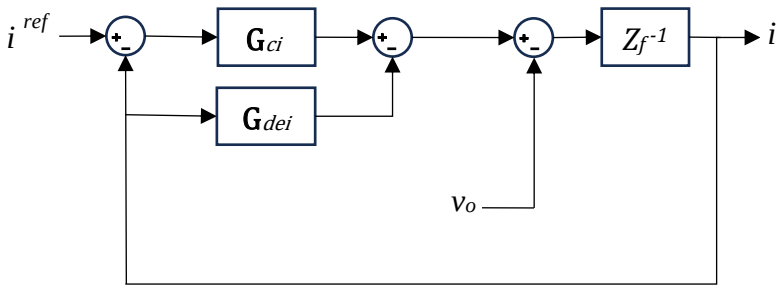

Figure 1.3 Block diagram of the transfer function of the system without considering PLL

Looking at this block diagram, it is evident that the output current is calculated with a combination of the output voltage and the reference value of the current. The goal is to calculate the output impedance of the VSC. Given the linearity of the system, the superposition rule can be applied. By assuming $i^{ref} = \begin{bmatrix} i_d^{ref} \\ i_q^{ref} \end{bmatrix} = 0$, the impedance of the VSC is calculated as in (1.14).

$$i = -Z_f^{-1} v_o + Z_f^{-1}(\mathbf{G}_{ci}(i^{ref} - i) - \mathbf{G}_{dei} i) \tag{1.14}$$

$$Z_{vsc} = \frac{v_o}{i} = -\left(Z_f + \mathbf{G}_{ci} + \mathbf{G}_{dei}\right) = -\begin{bmatrix} sL_f + R_f + k_p + \frac{k_i}{s} & 0 \\ 0 & sL_f + R_f + k_p + \frac{k_i}{s} \end{bmatrix}$$

$$= \frac{1}{Y_{vsc}}$$

Note that since this model is linear, the resulting impedance is valid for a wide range of frequencies. In practice, the PWM switching frequencies should be considered and the impedance values are valid up to half the switching frequencies.

1.2.3 Effects of the PLL dynamics

In the grid following architecture, the inverter is set to follow the grid's angle and frequency. This is achieved by utilizing a synchronous reference frame PLL. In power systems, PLL is a control mechanism that helps in synchronizing a local signal, typically a voltage of frequency, with a reference value that is often obtained from the grid. The control block diagram of a PLL is depicted in Figure 1.4. where k_p^{PLL} and k_i^{PLL} denote the PLL controller coefficients. In an inverter, the voltage is in the abc frame. First, this signal needs to be transformed to either the $\alpha\beta$ frame using Clark's transformation or the synchronous reference frame using the dq (Park's) transformation. The PLL ensures the proper operation of the inverter by ensuring that the two reference frames, the grid, and the control, are perfectly aligned.

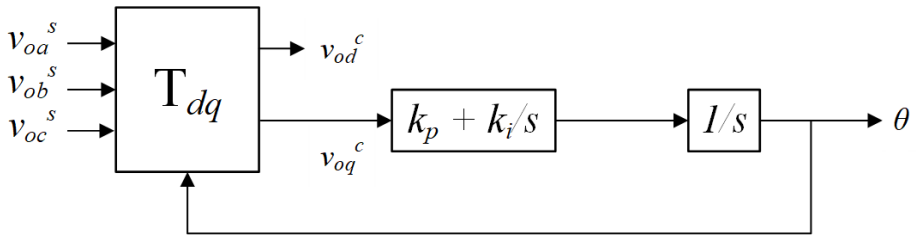

Figure 1.4 Schematic of synchronous reference frame PLL

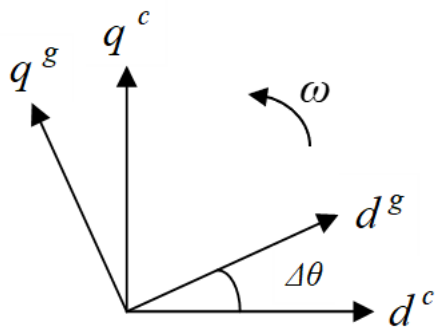

Figure 1.5 dq synchronous reference frames of the system and the controller

Once a small disturbance in the grid's voltage occurs, this perturbation is transferred to the inverter through the dynamics of the PLL. This results in two different dq axes: the grid and the PLL. The grid's frame is called "system", and denote it with the superscript s, and the PLL frame is called the controller frame, denoted by the superscript c. The phase difference between the two frames is depicted in Figure 1.5. In steady state, the two frames are aligned and there is no angle difference between them ($\Delta\theta = 0$). The steady-state values in the controller frame and the system frame for the input voltage of the inverter, its output voltage, and its current are depicted with capital letters in (1.15). where V_{id}^{c}, V_{iq}^{c}, V_{id}^{s}, and V_{iq}^{s} are the input voltage steady-state values for the controller dq frame and the system dq frame, and similarly, V_{od}^{c}, V_{oq}^{c}, V_{od}^{s}, and V_{oq}^{s} the steady-state output voltage values. Also, I_{d}^{c}, I_{q}^{c}, I_{d}^{s}, and I_{q}^{s} are the steady-state currents in the controller dq frame and the system dq frame, respectively.

$$\begin{bmatrix} V_{id}^{c} \\ V_{iq}^{c} \end{bmatrix} = \begin{bmatrix} V_{id}^{s} \\ V_{iq}^{s} \end{bmatrix}; \begin{bmatrix} V_{od}^{c} \\ V_{oq}^{s} \end{bmatrix} = \begin{bmatrix} V_{od}^{s} \\ V_{oq}^{s} \end{bmatrix}; \begin{bmatrix} I_{d}^{c} \\ I_{q}^{c} \end{bmatrix} = \begin{bmatrix} I_{d}^{s} \\ I_{q}^{s} \end{bmatrix} \tag{1.15}$$

Once a disturbance occurs, the difference between the two signals in the system frame and the controller frame is modelled using a transformation matrix $T_{\Delta\theta}$, as shown in (1.16). In the inverter control, this transformation is utilized to convert the grid's signal to a frame that is aligned with the inverter's controller frame.

$$T_{\Delta\theta} = \begin{bmatrix} cos(\Delta\theta) & sin(\Delta\theta) \\ -sin(\Delta\theta) & cos(\Delta\theta) \end{bmatrix} \tag{1.16}$$

As is evident, this transformation is highly nonlinear and is suitable for large signal analysis. To conduct a small-signal analysis, first we calculate the nominal operating points that were discussed in (1.15). Then, assuming the angle perturbation $\Delta\theta$ is small, the relationship between the controller and system frame signals can be linearized in the presence of small perturbations, as shown in (1.17), (1.18), and (1.19) where Δ denotes the small-signal perturbations.:

$$\begin{bmatrix} V_{id}^{c} + \Delta v_{id}^{c} \\ V_{iq}^{c} + \Delta v_{iq}^{c} \end{bmatrix} = \underbrace{\begin{bmatrix} 1 & \Delta\theta \\ -\Delta\theta & 1 \end{bmatrix}}_{T_{\Delta\theta}} \begin{bmatrix} V_{id}^{s} + \Delta v_{id}^{s} \\ V_{iq}^{s} + \Delta v_{iq}^{s} \end{bmatrix} \tag{1.17}$$

$$\begin{bmatrix} V_{od}^{c} + \Delta v_{od}^{c} \\ V_{oq}^{c} + \Delta v_{oq}^{c} \end{bmatrix} = \begin{bmatrix} 1 & \Delta\theta \\ -\Delta\theta & 1 \end{bmatrix} \begin{bmatrix} V_{od}^{s} + \Delta v_{od}^{s} \\ V_{oq}^{s} + \Delta v_{oq}^{s} \end{bmatrix} \tag{1.18}$$

$$\begin{bmatrix} I_{d}^{c} + \Delta i_{d}^{c} \\ I_{q}^{c} + \Delta i_{q}^{c} \end{bmatrix} = \begin{bmatrix} 1 & \Delta\theta \\ -\Delta\theta & 1 \end{bmatrix} \begin{bmatrix} I_{d}^{s} + \Delta i_{d}^{s} \\ I_{q}^{s} + \Delta i_{q}^{s} \end{bmatrix} \tag{1.19}$$

Since the steady state values of the system and controller are equal, these relations can be further simplified. Equation (1.20) shows an example of this simplification:

$$\begin{bmatrix} \Delta v_{id}^{c} \\ \Delta v_{iq}^{c} \end{bmatrix} \approx \begin{bmatrix} \Delta v_{id}^{s} + \Delta\theta V_{iq}^{s} \\ \Delta v_{iq}^{s} - \Delta\theta V_{id}^{s} \end{bmatrix} \tag{1.20}$$

Next, PLL dynamics are added separately. The block diagram representation of the PLL is depicted in 1.4. Based on this diagram, grid voltage in the abc frame is first transferred to the dq frame and using a PI controller, the angle difference is estimated.
Based on this representation, the output angle of the PLL is written as in (1.21).

$$\Delta\theta = (k_p^{PLL}\Delta v_{oq}^{c} + k_i^{PLL}\int \Delta v_{oq}^{c} dt)\frac{1}{s} \tag{1.21}$$

To write this system in the state space form, an auxiliary variable $\Delta\psi$ is defined, and the resulting state space is written in (1.22)

$$\Delta\psi = \int \Delta v_{oq}^{c} dt \tag{1.22}$$

$$\frac{d}{dt}\begin{bmatrix} \Delta\theta \\ \Delta\psi \end{bmatrix} = \begin{bmatrix} 0 & k_i^{PLL} \\ 0 & 0 \end{bmatrix}\begin{bmatrix} \Delta\theta \\ \Delta\psi \end{bmatrix} - \begin{bmatrix} 0 & k_p^{PLL} \\ 0 & 1 \end{bmatrix}\begin{bmatrix} \Delta v_{od}^{c} \\ \Delta v_{oq}^{c} \end{bmatrix} \tag{1.23}$$

Again, to get a uniform state space, the control frame signals are moved to the system frame as discussed before, with the transformation in (1.24).

$$\begin{bmatrix} \Delta v_{od}^{c} \\ \Delta v_{oq}^{c} \end{bmatrix} \approx \begin{bmatrix} \Delta v_{od}^{s} + \Delta\theta V_{oq}^{s} \\ \Delta v_{oq}^{s} - \Delta\theta V_{od}^{s} \end{bmatrix} \tag{1.24}$$

The resulting state space of the PLL in the controller frame is stated in (1.25).

$$\underbrace{\frac{d}{dt}\begin{bmatrix}\Delta\theta\\ \Delta\psi\end{bmatrix}}_{\dot{X}} = \underbrace{\begin{bmatrix}-k_p^{PLL}V_{od}^s & k_i^{PLL}\\ -V_{od}^s & 0\end{bmatrix}}_{A}\underbrace{\begin{bmatrix}\Delta\theta\\ \Delta\psi\end{bmatrix}}_{X} + \underbrace{\begin{bmatrix}0 & k_p^{PLL}\\ 0 & 1\end{bmatrix}}_{B}\underbrace{\begin{bmatrix}\Delta v_{od}^c\\ \Delta v_{oq}^c\end{bmatrix}}_{u} \tag{1.25}$$

1.2.4 The transfer function model with PLL dynamics

In this section the small signal representation of the system is derived in the block diagram form. This is buildup on the block diagram that was derived in section 1.2.21.2.2, where the PLL dynamics are added according to the derivation of section 1.2.3. To do so, the system frame signals, including the voltage and the current are transformed to the control stage. Finally, the input voltage of the controller which is in the control frame is transformed to the system frame.

The relationship between the output level voltage of the system is transformed to the system level, as stated in (1.26) and (1.27).

$$\begin{bmatrix}V_{od}^c + \Delta v_{od}^c\\ V_{oq}^c + \Delta v_{oq}^c\end{bmatrix} = \begin{bmatrix}1 & \Delta\theta\\ -\Delta\theta & 1\end{bmatrix}\begin{bmatrix}V_{od}^s + \Delta v_{od}^s\\ V_{oq}^s + \Delta v_{oq}^s\end{bmatrix} \tag{1.26}$$

$$\begin{bmatrix}\Delta v_{od}^c\\ \Delta v_{oq}^c\end{bmatrix} \approx \begin{bmatrix}\Delta v_{od}^s + V_{oq}^s\Delta\theta\\ \Delta v_{oq}^s - V_{od}^s\Delta\theta\end{bmatrix} \tag{1.27}$$

Next, based on the block diagram of the PLL, the relationship between the voltage and the angle is written as in (1.28), in which an auxiliary variable $\mathbf{T}_{PLL}$ is introduced to simplify the relations.

$$\Delta\theta = \Delta v_{oq}^c.\underbrace{(k_p^{PLL} + \frac{k_i^{PLL}}{s}).\frac{1}{s}}_{\mathbf{T}_{PLL}} = \Delta v_{oq}^c.\mathbf{T}_{PLL} \tag{1.28}$$

$$\Delta v_{od}^c = \Delta v_{od}^s + V_{oq}^s.\Delta v_{oq}^c.\mathbf{T}_{PLL} \tag{1.29}$$

$$\Delta v_{oq}^c = \Delta v_{oq}^s - V_{od}^s.\Delta v_{oq}^c.\mathbf{T}_{PLL} \tag{1.30}$$

By further simplifying (1.30), (1.31) is derived.

$$(1 + V_{od}^s\mathbf{T}_{PLL})\Delta v_{oq}^c = \Delta v_{oq}^s \tag{1.31}$$

Inserting (1.31) into (1.29), (1.32) is derived.

$$\Delta v_{od}^c = \Delta v_{od}^s + V_{oq}^s\left(\frac{1}{1 + V_{od}^s\mathbf{T}_{PLL}}\right)\Delta v_{oq}^s \tag{1.32}$$

These relations are summarized in the transformation matrix form, depicted in (1.33)

$$\begin{bmatrix}\Delta v_{od}^{c}\\ \Delta v_{oq}^{c}\end{bmatrix}=\begin{bmatrix}1 & \dfrac{V_{oq}^{s}\mathbf{T}_{PLL}}{1+V_{od}^{s}\mathbf{T}_{PLL}}\\ 0 & \dfrac{1}{1+V_{od}^{s}\mathbf{T}_{PLL}}\end{bmatrix}\begin{bmatrix}\Delta v_{od}^{s}\\ \Delta v_{oq}^{s}\end{bmatrix} \tag{1.33}$$

The same procedure is repeated for the output current, and the relationship is written in (1.36), in which the controller frame current perturbations are written as a function of grid frame voltages, because of PLL dynamics. The transfer function $\mathbf{T}_{vi}$ transforms the grid's voltage signals to the current signals.

$$\begin{bmatrix}I_{d}^{c}+\Delta i_{d}^{c}\\ I_{q}^{c}+\Delta i_{q}^{c}\end{bmatrix}=\begin{bmatrix}1 & \Delta\theta\\ -\Delta\theta & 1\end{bmatrix}\begin{bmatrix}I_{d}^{s}+\Delta i_{d}^{s}\\ I_{q}^{s}+\Delta i_{q}^{s}\end{bmatrix} \tag{1.34}$$

$$\begin{bmatrix}\Delta i_{d}^{c}\\ \Delta i_{q}^{c}\end{bmatrix}\approx\begin{bmatrix}\Delta i_{d}^{s}+I_{q}^{s}\Delta\theta\\ \Delta i_{q}^{s}-I_{d}^{s}\Delta\theta\end{bmatrix} \tag{1.35}$$

$$\begin{bmatrix}\Delta i_{d}^{c}\\ \Delta i_{q}^{c}\end{bmatrix}=\begin{bmatrix}\Delta i_{d}^{s}\\ \Delta i_{q}^{s}\end{bmatrix}+\underbrace{\begin{bmatrix}0 & \dfrac{I_{q}^{s}\mathbf{T}_{PLL}}{1+V_{od}^{s}\mathbf{T}_{PLL}}\\ 0 & -\dfrac{I_{d}^{s}\mathbf{T}_{PLL}}{1+V_{od}^{s}\mathbf{T}_{PLL}}\end{bmatrix}}_{\mathbf{T}_{vi}}\begin{bmatrix}\Delta v_{od}^{s}\\ \Delta v_{oq}^{s}\end{bmatrix} \tag{1.36}$$

Repeating a similar procedure, the input voltage of the inverter is transformed from the control frame to the system frame, as stated in (1.39). Similarly, the transfer function T_{vv} transforms the grid's output voltage signals to the input voltages in system frame.

$$\begin{bmatrix}V_{id}^{c}+\Delta v_{id}^{c}\\ V_{iq}^{c}+\Delta v_{iq}^{c}\end{bmatrix}=\begin{bmatrix}1 & \Delta\theta\\ -\Delta\theta & 1\end{bmatrix}\begin{bmatrix}V_{id}^{s}+\Delta v_{id}^{s}\\ V_{iq}^{s}+\Delta v_{iq}^{s}\end{bmatrix} \tag{1.37}$$

$$\begin{bmatrix}\Delta v_{id}^{c}\\ \Delta v_{iq}^{c}\end{bmatrix}\approx\begin{bmatrix}\Delta v_{id}^{s}+V_{iq}^{s}\Delta\theta\\ \Delta v_{iq}^{s}-V_{id}^{s}\Delta\theta\end{bmatrix} \tag{1.38}$$

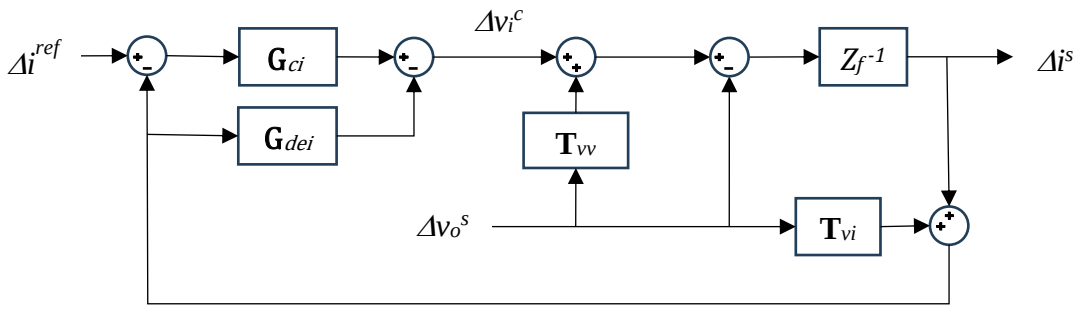

Figure 1.6 Block diagram of the transfer function of system with PLL dynamics

$$\begin{bmatrix}\Delta v_{id}^{s}\\ \Delta v_{iq}^{s}\end{bmatrix} \approx \begin{bmatrix}\Delta v_{id}^{c}\\ \Delta v_{iq}^{c}\end{bmatrix} + \underbrace{\begin{bmatrix}0 & -\dfrac{V_{iq}^{s}\mathbf{T}_{PLL}}{1+V_{od}^{s}\mathbf{T}_{PLL}}\\ 0 & \dfrac{V_{id}^{s}\mathbf{T}_{PLL}}{1+V_{od}^{s}\mathbf{T}_{PLL}}\end{bmatrix}}_{T_{vv}}\begin{bmatrix}\Delta v_{od}^{s}\\ \Delta v_{oq}^{s}\end{bmatrix} \tag{1.39}$$

Now that the relationships between the controller frame and the grid frame is derived, these transformations are put together to form the block diagram of the system, as depicted in Figure 1.6.

This is a MIMO system with inputs $[\Delta i_d^{ref}, \Delta i_q^{ref}, \Delta v_d^s, \Delta v_q^s]$ and the output $[\Delta i_d^s, \Delta i_q^s]$. Based on this block diagram and using the superposition rule, the output admittance of the system is calculated as presented in (1.41), where the components of this admittance are stated in (1.42), (1.43), (1.44), and (1.45).

$$\frac{\Delta i^s}{\Delta v_o^s} = \frac{-\mathbf{I} - (\mathbf{G}_{ci} + \mathbf{G}_{dei})\mathbf{T}_{vi} + \mathbf{T}_{vv}^{PLL}}{Z_f + \mathbf{G}_{ci} + \mathbf{G}_{dei}} \tag{1.40}$$

$$Y_{vsc} = \begin{bmatrix}-\dfrac{s}{\sigma_2} & -\dfrac{\sigma_3}{\sigma_1}\\ 0 & \dfrac{\sigma_4}{\sigma_1}\end{bmatrix} \tag{1.41}$$

$$\sigma_1 = \left(s^2 + V_{od}^s k_p^{PLL} s + V_{od}^s k_i^{PLL}\right)\sigma_2 \tag{1.42}$$

$$\sigma_2 = k_i + (R_f + k_p)s + L_f s^2 \tag{1.43}$$

$$\sigma_3 = I_q^s k_i k_i^{PLL} + (V_{iq}^s k_i^{PLL} + I_q^s k_i k_p^{PLL} + I_q^s k_p k_i^{PLL} - I_d^s L_f k_i^{PLL}\omega)s + (V_{iq}^s k_p^{PLL} + I_q^s k_p k_p^{PLL} - I_d^s L_f k_p^{PLL}\omega)s^2 \quad (1.44)$$

$$\sigma_4 = I_d^s k_i k_i^{PLL} + (V_{id}^s k_i^{PLL} - V_{od}^s k_i^{PLL} + I_d^s k_i k_i^{PLL} + I_d^s k_p k_i^{PLL} + I_q^s L_f k_i^{PLL}\omega)s^2 - s^3 \quad (1.45)$$

1.3 Impedance-based stability analysis

Once the impedance of the inverter is derived, this can be used to study the impacts of different parameters on the grid synchronization stability of the inverters. That is because the behavior of the inverter in a spectrum of frequencies can accurately be captured by its impedance. To this end, the impedance-based stability analysis is used. The main idea of this method is to divide a system into two subsystems, one being the element under study and two the rest of the power grid, as shown in Figure 1.7, provided that each of them is independently stable. This stability analysis is also known as the impedance ratio analysis. The grid and the inverter impedances are represented in the format of Figure 1.8, and denoted by Z_g for the grid and Z_{vsc} for the converter. Assuming that the system is a SISO, using the function $1 + \frac{Z_g}{Z_{vsc}}$ it is possible to assess the stability. This criterion states that if this transfer function has no zeros in the closed right half plane, then the system is stable. This is based on the Nyquist theorem (which will be elaborated on in the following section), where the number of closed right half plane zeros is equal to the number of encirclements of the function $\frac{Z_g}{Z_{vsc}}$ around the point $(-1, j0)$. This condition is satisfied if for all frequencies, the magnitude of the grid's impedance is smaller than the magnitude of the inverter's impedance, as stated in (1.46), implying that the grid must be strong.

$$\left\|Z_g(j\omega)\right\| < \|Z_{vsc}(j\omega)\| \quad (1.46)$$

Consider an inverter that is simplified as a current source I_{vsc} parallel with an impedance Z_{vsc}, connected to a grid that is modelled by a voltage source V_g series with an impedance Z_g. The goal is to assess whether the flow of current *I* between the two systems remains stable or not.
Writing a KCL to find the current gives the equation) 1.48).

$$I(s) = \frac{I_{vsc}Z_{vsc}}{Z_{vsc} + Z_g} - \frac{V_g}{Z_{vsc} + Z_g} \quad (1.48)$$

Simplifying this results in (1.49).

$$I(s) = [I_{vsc} - \frac{V_g}{Z_{vsc}}] \times \frac{1}{1 + \frac{Z_g}{Z_{vsc}}} \quad (1.49)$$

The first term of the equation can be assumed to be stable. Now, for the interconnected system to be stable, the stability of the second term must be investigated.

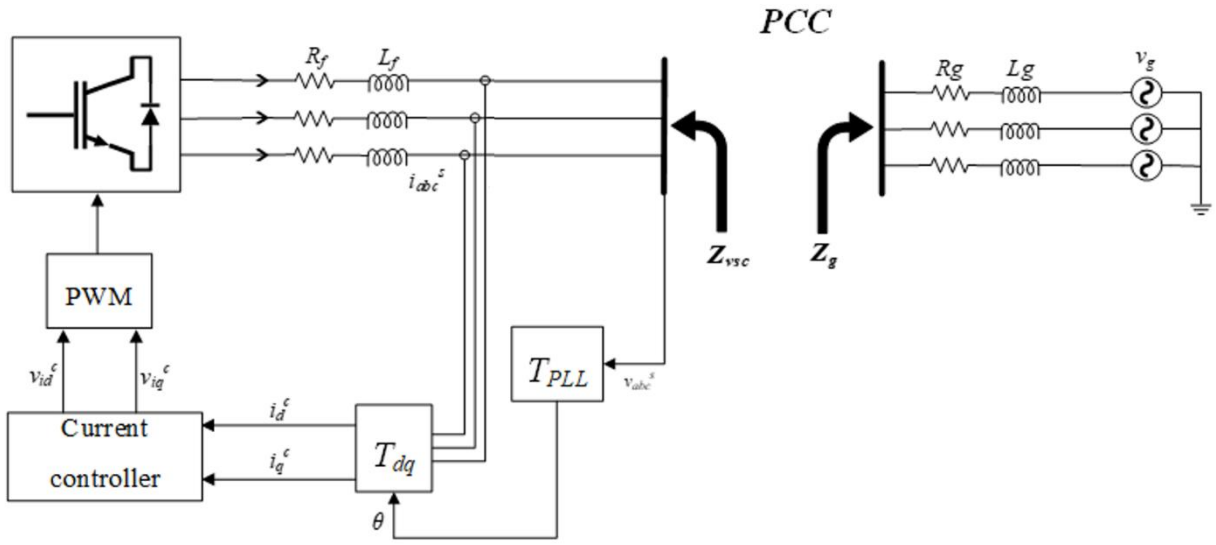

Figure 1.7 Schematic of the impedance based modeling of the grid connected VSC

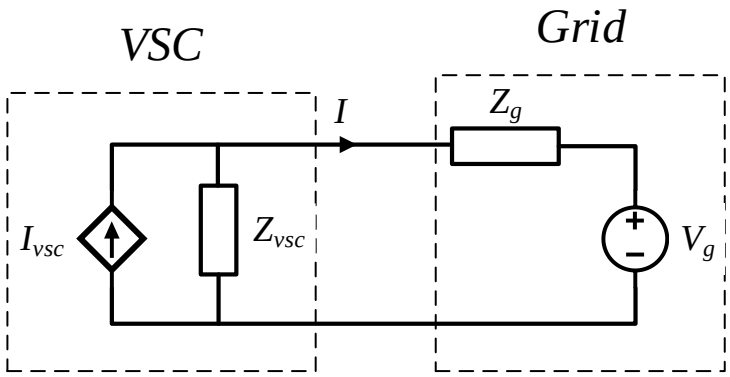

Figure 1.8 Schematic of the interconnection of the grid and VSC equivalents

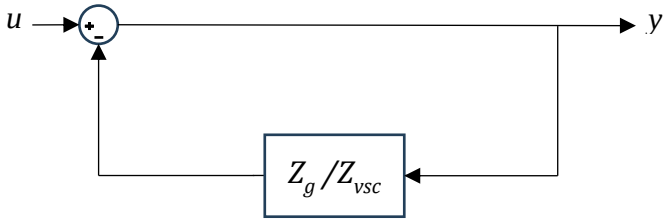

Figure 1.9 Representation of impedance stability analysis as a closed loop system

This term perfectly fits the application of the classic Nyquist stability criterion because the impedance ratio represents the open-loop gain, with the controller block diagram depicted in Figure 1.9. With this structure, classical control methods, like the Nyquist and bode plots could be applied to comment on the stability. But, since the impedance ratio is a matrix, which is due to the

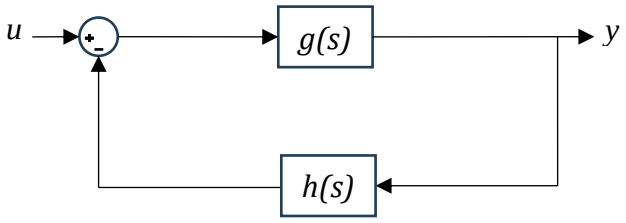

Figure 1.10 Generic model of SISO feedback system

MIMO structure of the system, the generalized version of the Nyquist criterion must be used. Next, we briefly discuss the principles of the Nyquist criterion in SISO systems and how it is extended to MIMO systems, which is the case of inverter stability analysis.

1.4 The Nyquist criterion: SISO to MIMO

In this section, we discuss the principles of using the Nyquist criterion on stability analysis of SISO linear time invariant systems. This criterion applies the *Cauchy's principle of argument* on the *open loop* transfer function of a system and from there, we can comment on the *closed loop* stability. Consider the closed loop transfer function of the feedback system in Figure 1.10, as stated in (1.50).

$$m(s) = \frac{g(s)}{1 + g(s)h(s)} \tag{1.50}$$

The closed loop poles of the system are achieved by finding the zeros of (1.51), which is called the system characteristic equation.

$$d(s) = 1 + g(s)h(s) \tag{1.51}$$

Now, to derive the Nyquist plot, one can create the closed region in the s-plane as shown in Figure 1.11, and find the mapping of the function $d(s) = 1 + g(s)h(s)$ whose zeros are the closed-loop poles of the transfer function.
The number of unstable closed-loop poles is equal to the number of unstable open-loop poles, plus the number of encirclements of the origin of the Nyquist plot of the complex function $d(s)$.

$$N = Z - P \tag{1.52}$$

where Z and P stand for the number of zeros and poles of the function $d(s)$ inside the contour. The above criterion can be slightly modified if instead of plotting the function $d(s) = 1 + g(s)h(s)$ and counting the clockwise encirclement of the origin, we consider the function $g(s)h(s)$, and count the encirclements around the point $(-1, j0)$.

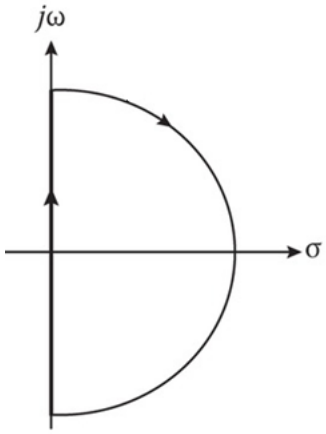

Figure 1.11 s-plane contour of the right half plane

To extend this concept to MIMO systems, first consider the generic 2×2 system as depicted in Figure 1.12, where $G = \begin{bmatrix} G_{11} & G_{12} \\ G_{21} & G_{22} \end{bmatrix}$ and $H = \begin{bmatrix} H_{11} & 0 \\ 0 & H_{22} \end{bmatrix}$. If there is no coupling between the channels ($G_{12} = G_{21} = 0$), the system turns into two independent SISO systems. To apply the Nyquist criterion to this MIMO system, we need to know the definition of poles and zeros in a MIMO system, which is acquired with the Smith-McMillan form of a transfer function matrix [12]. Once the number of poles and zeros are obtained, the collective encirclements of the loop gain eigenvalues are utilized to check for the Nyquist stability criterion.

The power system equivalent of this system is a 2×2 MIMO system, in which the loop gain has two eigenvalues λ_1 and λ_2. One important thing to consider is that the return ratio of the loop gain must be a rational function, meaning that the order of the numerator is less than the order of the denominator. If the two subsystems are modelled as Thevenin/Norton equivalents which leads to a $Z + Y$ connection, the resulting return ratio will always be rational. For models which result in a $Z + Z$ or $Y + Y$ representations, as depicted in Figure 1.13 for various combinations, alternative methods should be applied to assess the stability [13] One thing to note is that the representations in Figure 1.13 are equivalent, if $Y_{vsc} = Z_{vsc}^{-1}$ and $Y_g = Z_g^{-1}$.

1.5 Analysis of impacts of different parameters on the stability of the inverters

In this section, the impacts of different parameters such as the grid strength and parameters of the synchronization mechanism (i.e. PLL) on the stability of inverter is studies. First, bode plots for each element of the admittance and the impedance matrices are plotted. After that, the GNC plots for various grid strengths has been plotted to demonstrate how a weak grid results in an unstable interconnection. The parameters for this study have been summarized in the Table 1.

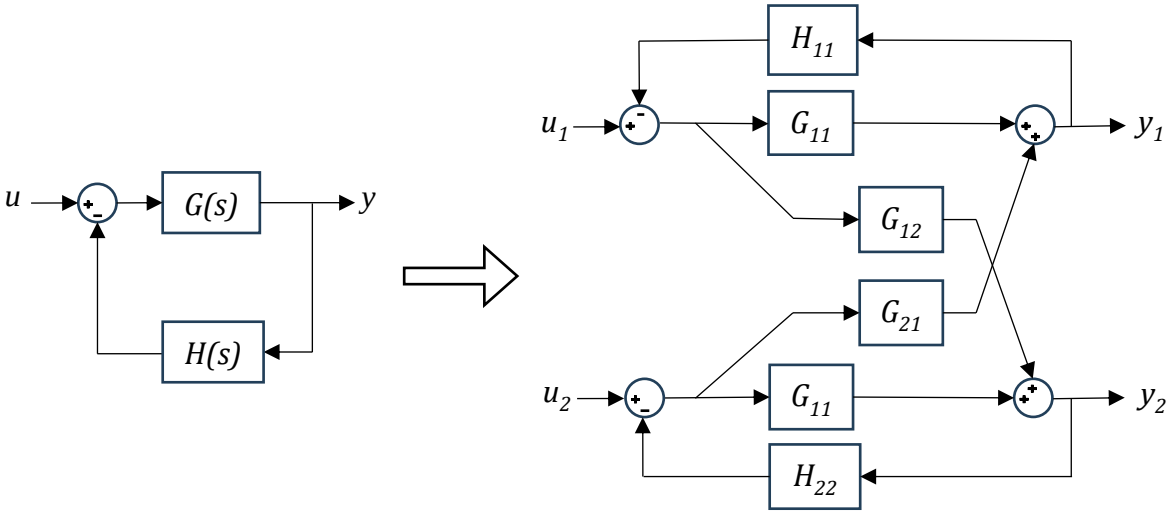

Figure 1.12 Schematic of a 2 × 2 MIMO system

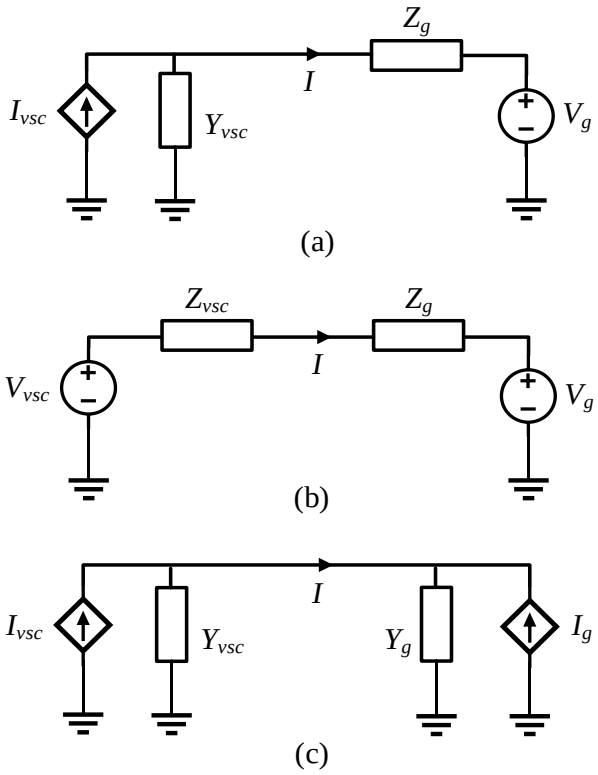

Figure 1.13 Different combinations of VSC and grid equivalent models

Table 1 Parameters of the VSC [10]

Parameter	Value
k_p	0.023
k_i	25.59
k_p^{PLL}	4.46, 8.92, 17.84
k_i^{PLL}	991, 3964, 15860
ω	$2\pi \times 60\ rad/s$
R_f	120 $m\Omega$
L_f	970 μH
I_d^s	-11 Amp
I_q^s	0 Amp
v_{id}^s	100 v
v_{iq}^s	0 v
v_{od}^s	99.9 v
v_{oq}^s	0 v

1.5.1 Results without considering the PLL dynamics

In this scenario, the impedance (admittance) matrix is purely diagonal, and the values are identical on each axis ($Z_{dd} = Z_{qq}$ and $Y_{dd} = Y_{qq}$). Consequently, only the output impedance and admittance of the VSC on one axis is plotted in Figure 1.14 and Figure 1.15, respectively.

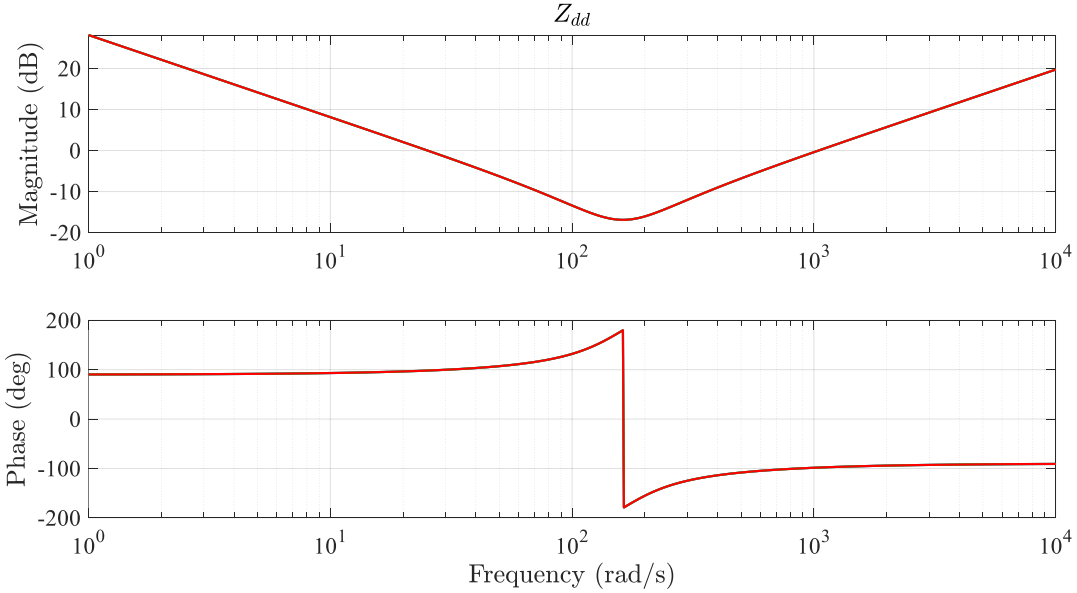

Figure 1.14 Z_{dd} impedance of the VSC in the absence of PLL dynamics

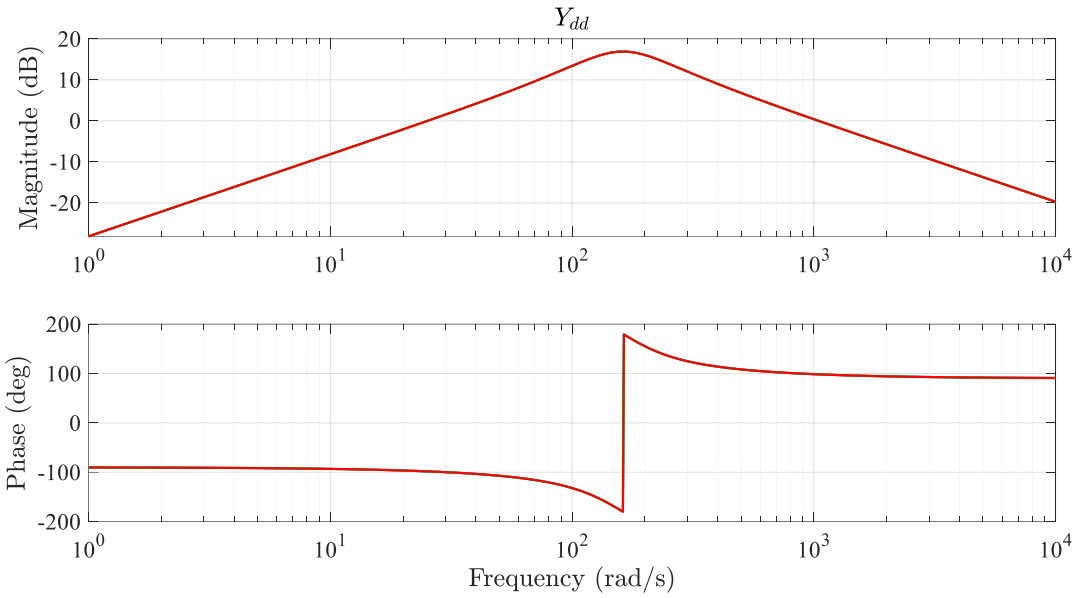

Figure 1.15 Y_{dd} admittance of the VSC in the absence of PLL dynamics

1.5.2 Impedance/admittance with the PLL dynamics

Once the PLL is added, the impedance matrix is no longer diagonal. Z_{dd} and Z_{qd} will be identical to the no PLL case, but Z_{dq} will no longer be zero. To further probe the effects of PLL, three different PLL coefficients are considered. The impedances and admittances of the VSC are depicted in Figure 1.16 to Figure 1.19. As depicted in Figure 1.16 the dq channel gain is relatively small. Figure 1.18 shows that while synchronizing a VSC with the grid, the qq channel behaves as a negative incremental resistance. This behavior is a result of including PLL dynamics, where the PLL bandwidth determines the frequency range at which the impedance is negative. For instance, $k_p^{PLL} = 4.46$ & $k_i^{PLL} = 991$, the negative impedance starts to damp out around 50 Hz with a relatively steep rate, but for $k_p^{PLL} = 17.84$ & $k_i^{PLL} = 15860$ this decrease happens with a lower slope and in higher frequencies.

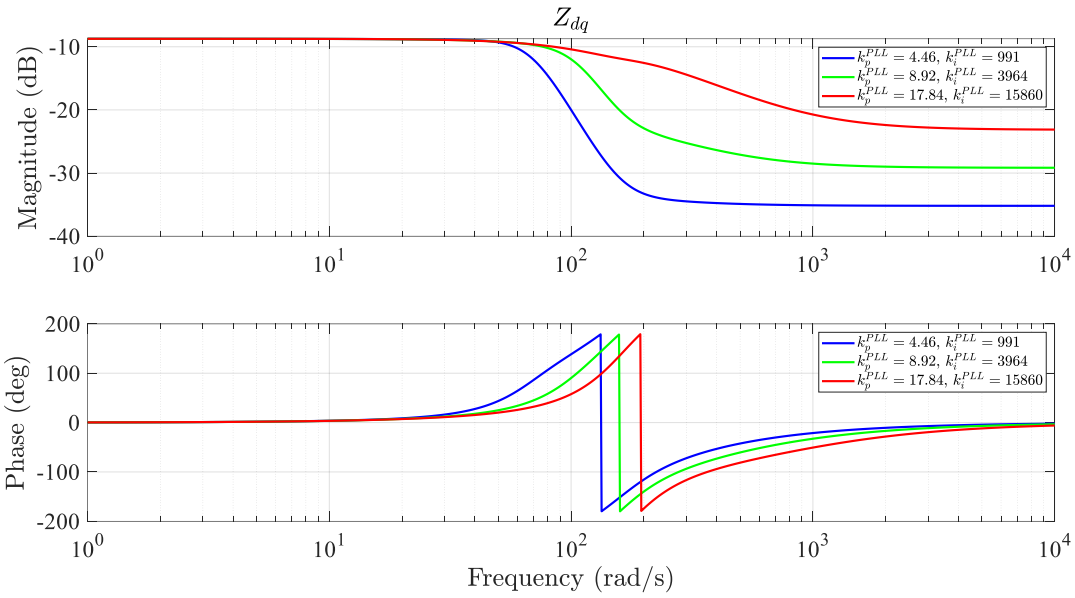

Figure 1.16 dq channel impedance of the VSC

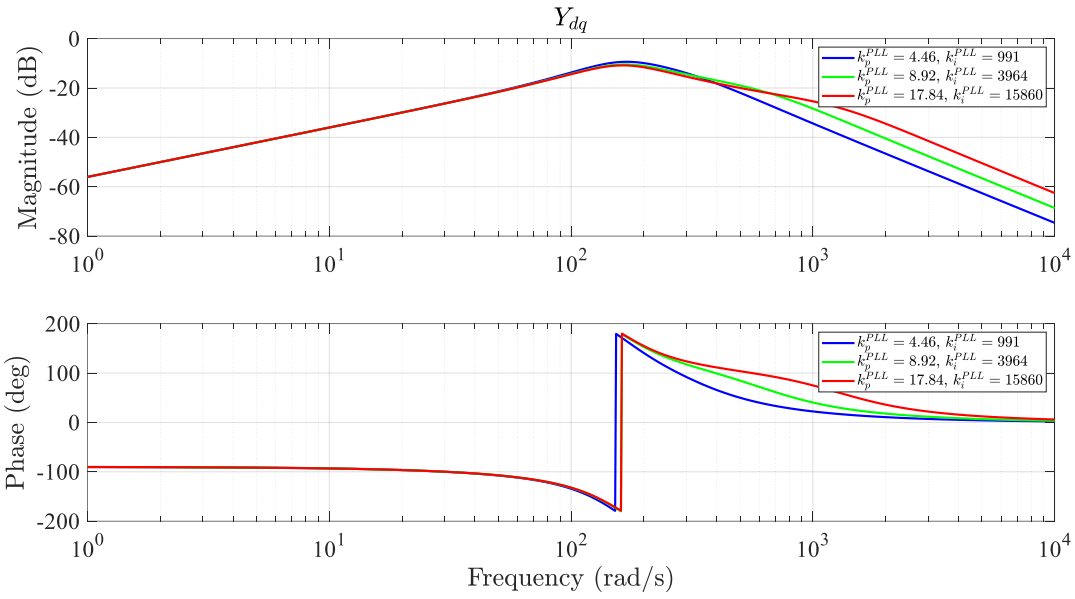

Figure 1.17 dq channel admittance of the VSC

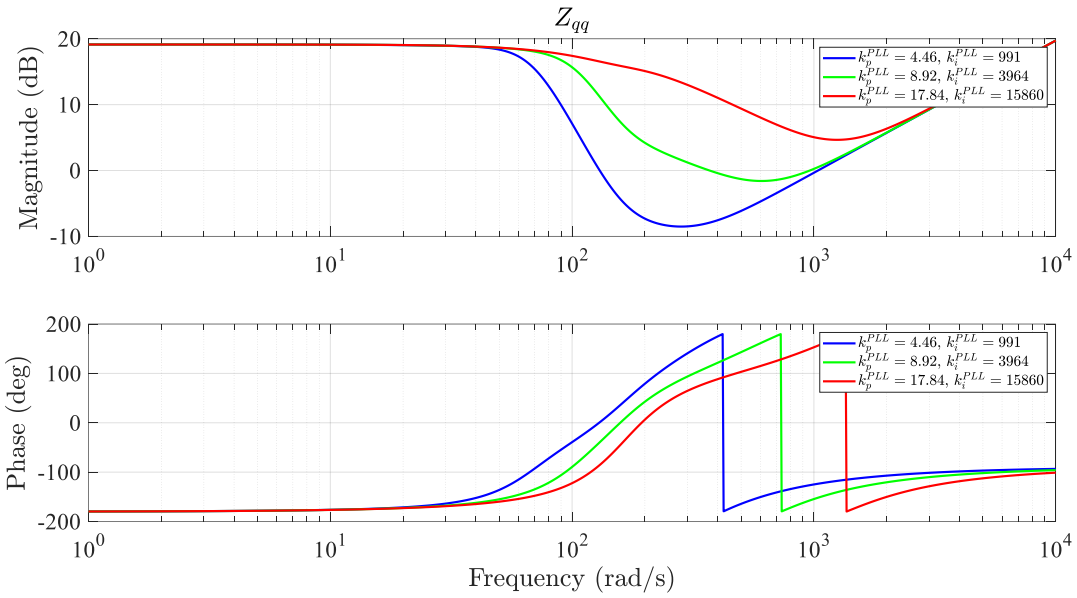

Figure 1.18 qq channel impedance of the VSC

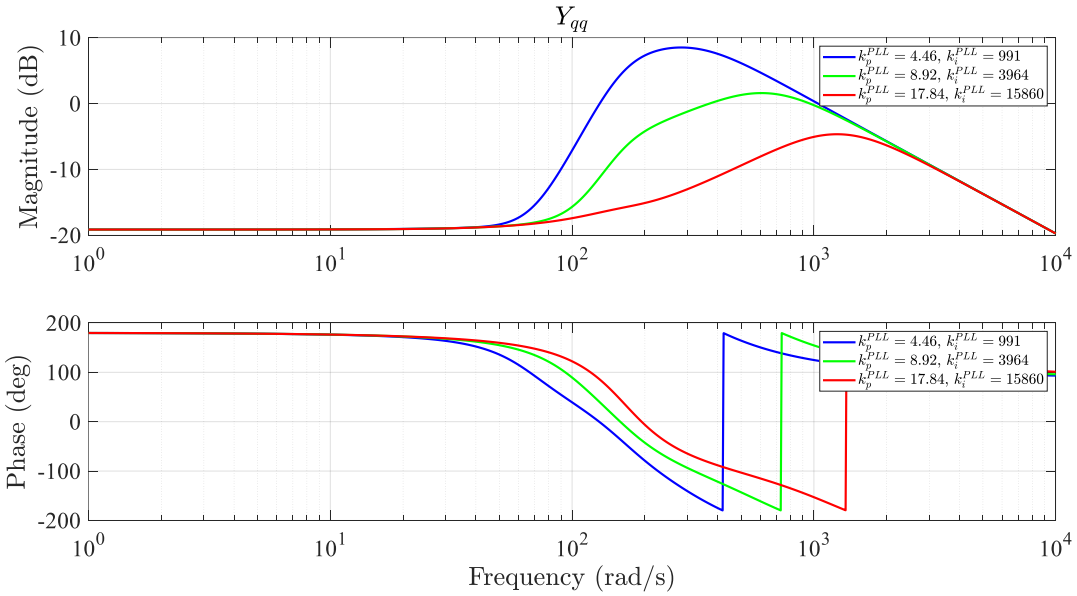

Figure 1.19 qq channel admittance of the VSC

1.5.3 Stability analysis using the GNC plots.

Generally, a power system's strength is related to the amount of available short circuit current in a certain part of the system, which affects its ability to recover from disturbances. The most common method to define the strength of the system at the point of injection (POI) of the inverter at is the short circuit ratio (SCR), which is the ratio of short circuit in a given location, to the rating of the source connected to that location. Accordingly, SCR is represented as follows:

$$SCR_{POI} = \frac{\text{SC } MVA_{POI}}{MW_{POI}} \tag{1.53}$$

Consequently, a strong grid has a high SCR and can maintain its voltage during disturbances. To demonstrate the impact of the grid strength on inverter stability the GNC plots are used. First, the inverter is connected to a power grid with $R_g = 0.08\,\Omega$ and $L_g = 8 \times 10^{-4}$ H. The GNC plot for this case is plotted in Figure 1.20. As depicted, none of the eigen loci graphs encircle the critical point $(-1,0j)$, which indicates that the system is stable. Then, as the strength of the grid is reduced by increasing its impedance as shown in Figure 1.21 and Figure 1.22, respectively, the loci graphs move towards the critical point and both encircle it, indicating the instability of the system in a weak grid connection.

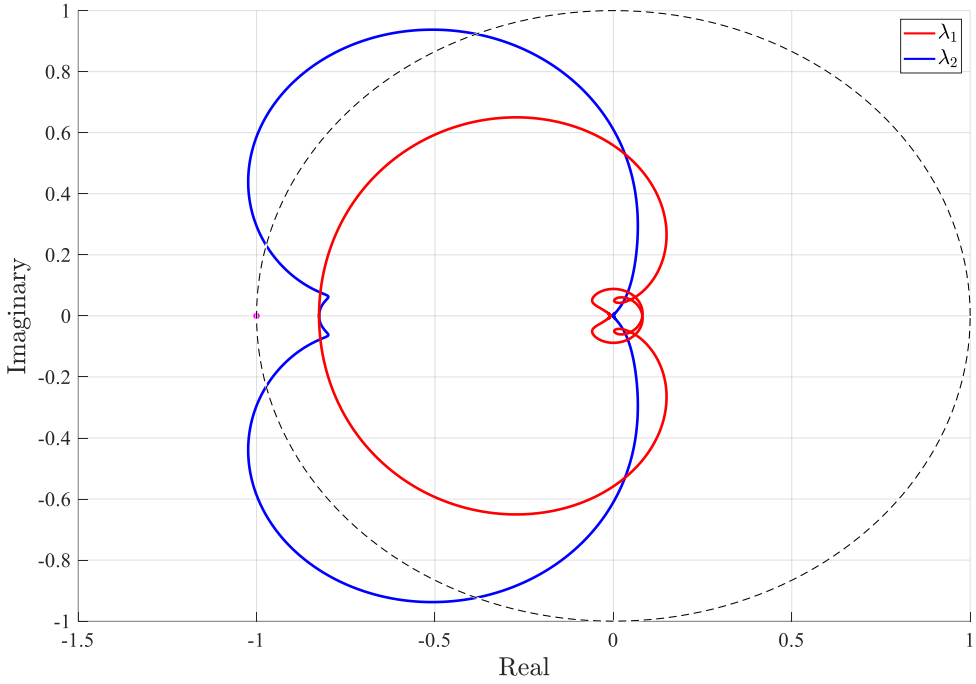

Figure 1.20 GNC plots for $R_g = 0.08\,\Omega$ and $L_g = 8 \times 10^{-4}$ H

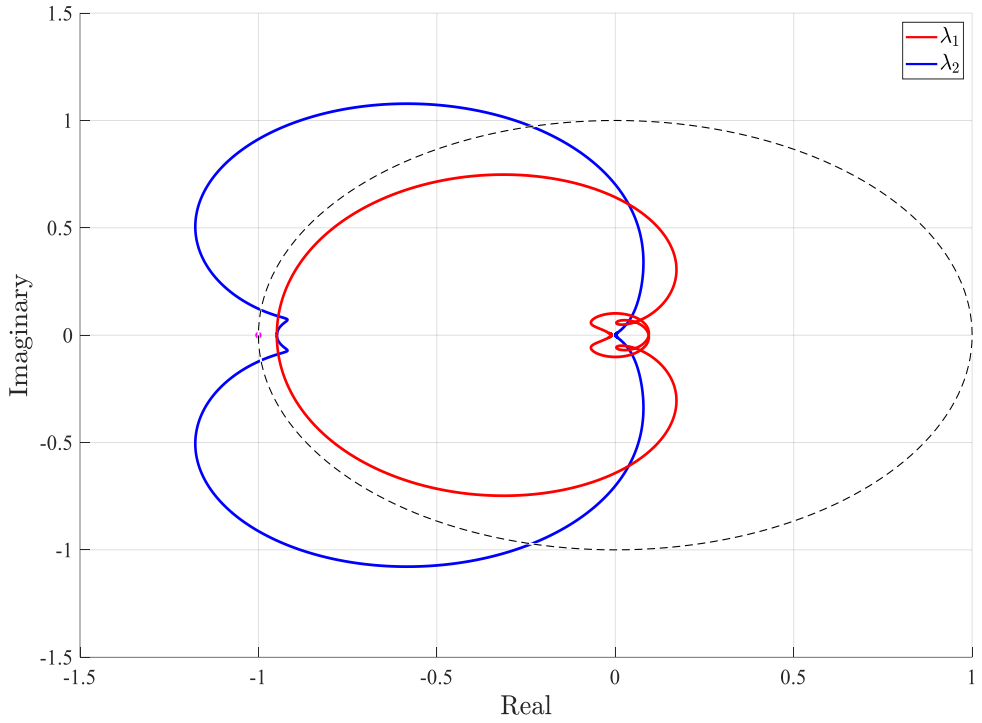

Figure 1.21 GNC plots for $R_g = 0.09\ \Omega$ and $L_g = 9 \times 10^{-4}$ H

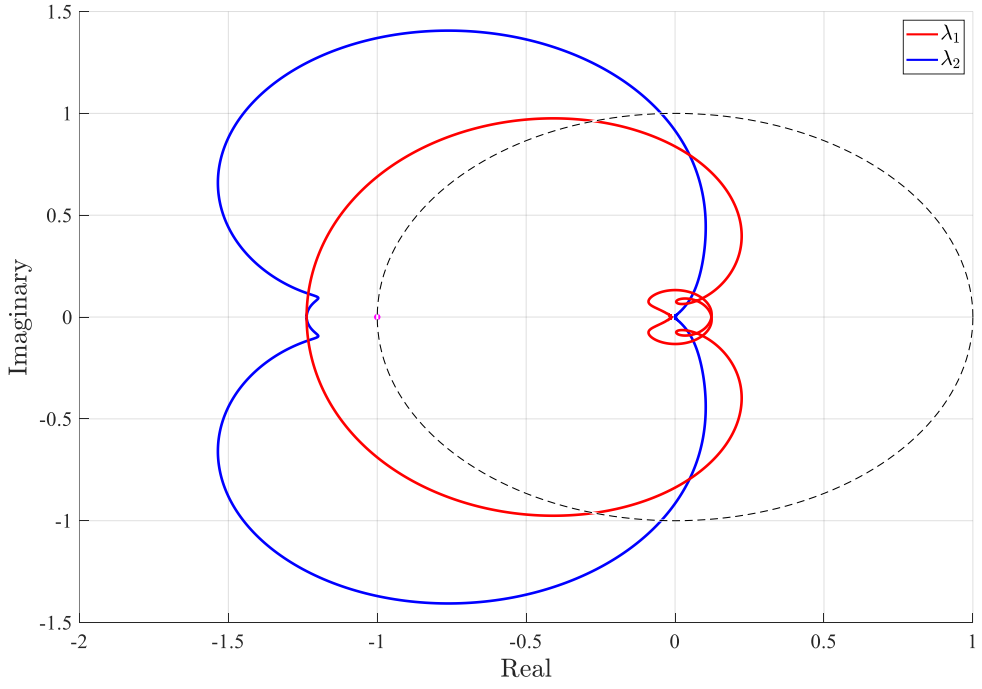

Figure 1.22 GNC plots for $R_g = 0.12\ \Omega$ and $L_g = 1.2 \times 10^{-3}$ H.

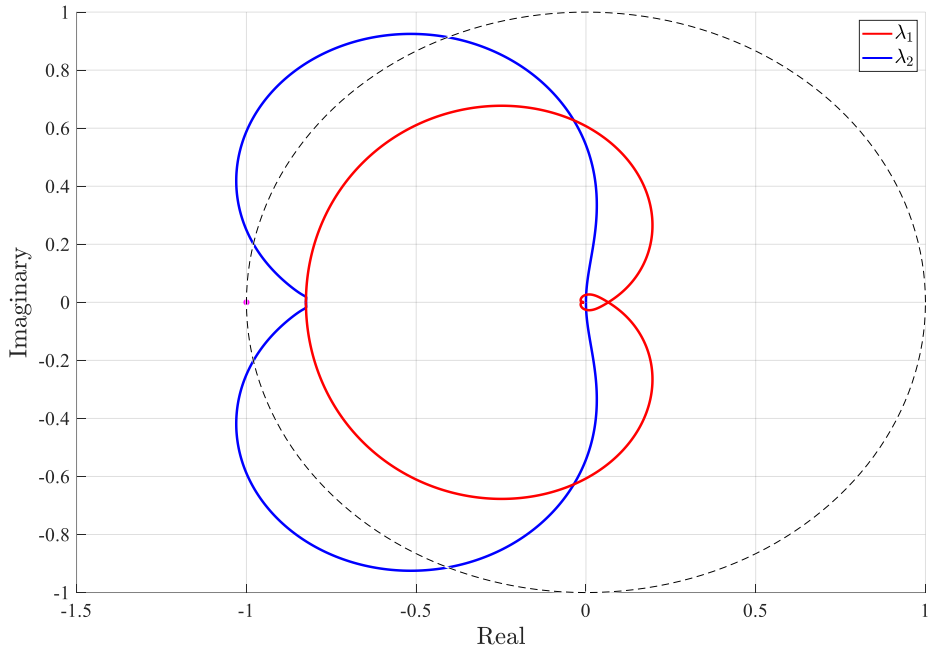

Figure 1.23 GNC plots ignoring the off-diagonals for $R_g = 0.08\ \Omega$ and $L_g = 8 \times 10^{-4}$ H.

In some studies, the off-diagonal elements of the 2×2 MIMO are ignored. Therefore, the stability analysis is simplified as the MIMO system becomes two independent SISO systems. For strong power grid this simplification is acceptable, but as it is shown later this simplification fails in a weak grid condition. First, consider the strong grid for which the GNC was depicted in Figure 1.20. Now, if the model is simplified by ignoring the off-diagonal elements, still the stability is reported correctly as shown in Figure 1.23.

Now consider a different case with $R_g = 0.092\ \Omega$ and $L_g = 9.2 \times 10^{-4}$ H and $k_p^{PLL} = 4.46$ and $k_i^{PLL} = 991$. The GNC plot of this case is depicted in Figure 1.24, and its simplified counterpart is depicted in Figure 1.25. The complete setup with a full matrix indicates the instability of the system, but the simplified setup wrongly reports that as stable.

Similarly, if from the start the PLL dynamics is not considered, a diagonal impedance as discussed in the modelling section is derived. It was already observed that $R_g = 0.092\ \Omega$ and $L_g = 9.2 \times 10^{-4}$ H represent a weak grid and the VSC interconnection with PLL dynamics is unstable. Figure 1.26 shows the result of applying the Nyquist criterion to the impedance model without the PLL dynamics, where the algorithm incorrectly indicates the stability.

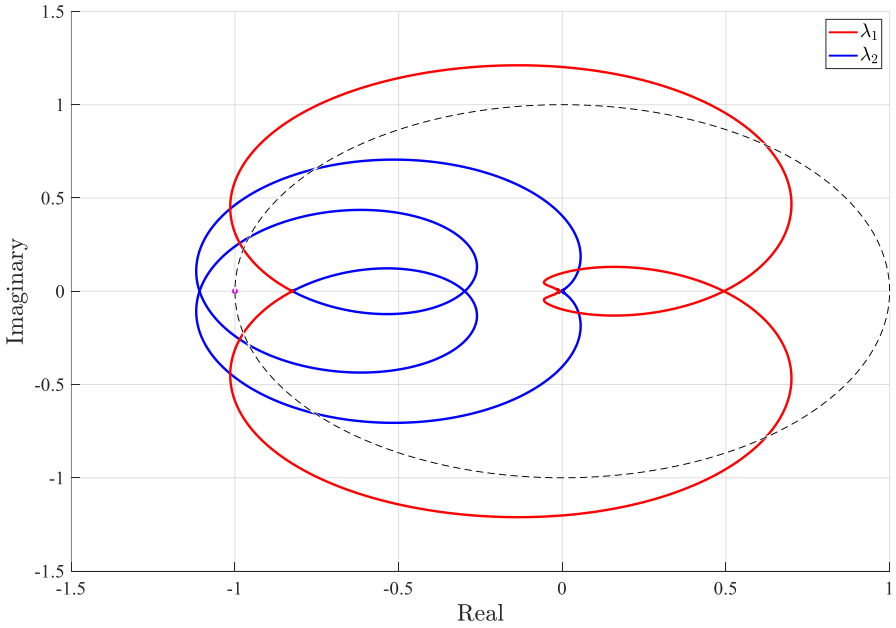

Figure 1.24 Complete and unstable case with $R_g = 0.092\ \Omega$ and $L_g = 9.2 \times 10^{-4}$ H and $k_p^{PLL} = 4.46$ and $k_i^{PLL} = 991$.

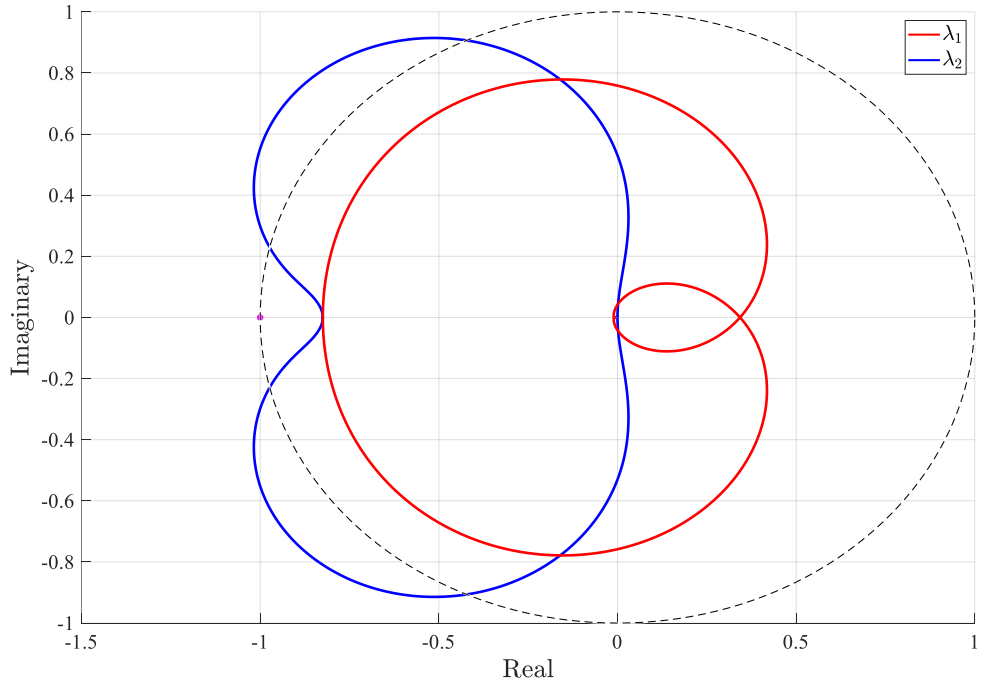

Figure 1.25 Simplified cased with $R_g = 0.092\ \Omega$ and $L_g = 9.2 \times 10^{-4}$ H and $k_p^{PLL} = 4.46$ and $k_i^{PLL} = 991$, wrongly reported as stable.

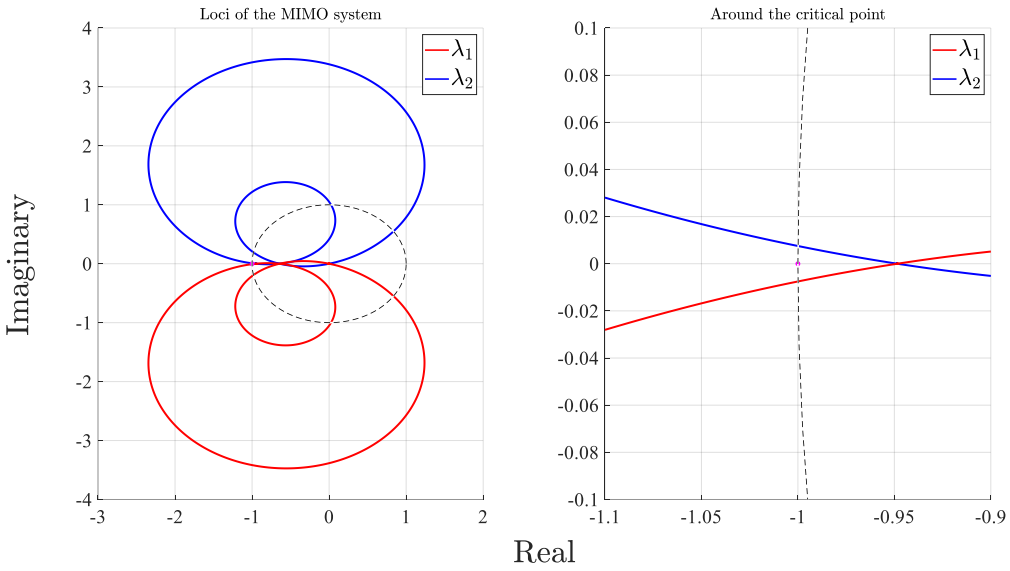

Figure 1.26 GNC for a weak grid while ignoring the PLL dynamics

1.6 Case study of impacts of line outages on grid synchronization stability of inverters

Once faults occur in power grids, due to the subsequent line outages and/or possible power system splitting, the strength of the system may reduce. The sudden reduction in the strength of the system may cause loss of grid synchronism of inverters. A real-world example of such a scenario occurred in 2017 in First Solar 550 MW utility-scale PV plant. Figure 1.27 shows an inverter connected to the power grid simulated in Matlab/Simulink. At t=0.3, the system becomes weaker by taken the parallel line out of service leading to SCR≈ 1. As shown in Figures 1.28 inverter lose its synchronization stability. As shown in Figures 1.29 by increasing the time response of PLL, grid synchronism stability of the IBR can be increased in facing sudden change in the strength of the system. However, slow PLL does not provide desirable response in tracking the fast change in the system quantities such as frequency of the grid during large disturbances. Therefore, alternative solutions should be proposed. Specifically, in the next section a supplementary controller is implemented to increasing the damping of the controllers so that output oscillations are damped out effectively which leads to increased grid synchronization of IBRs.

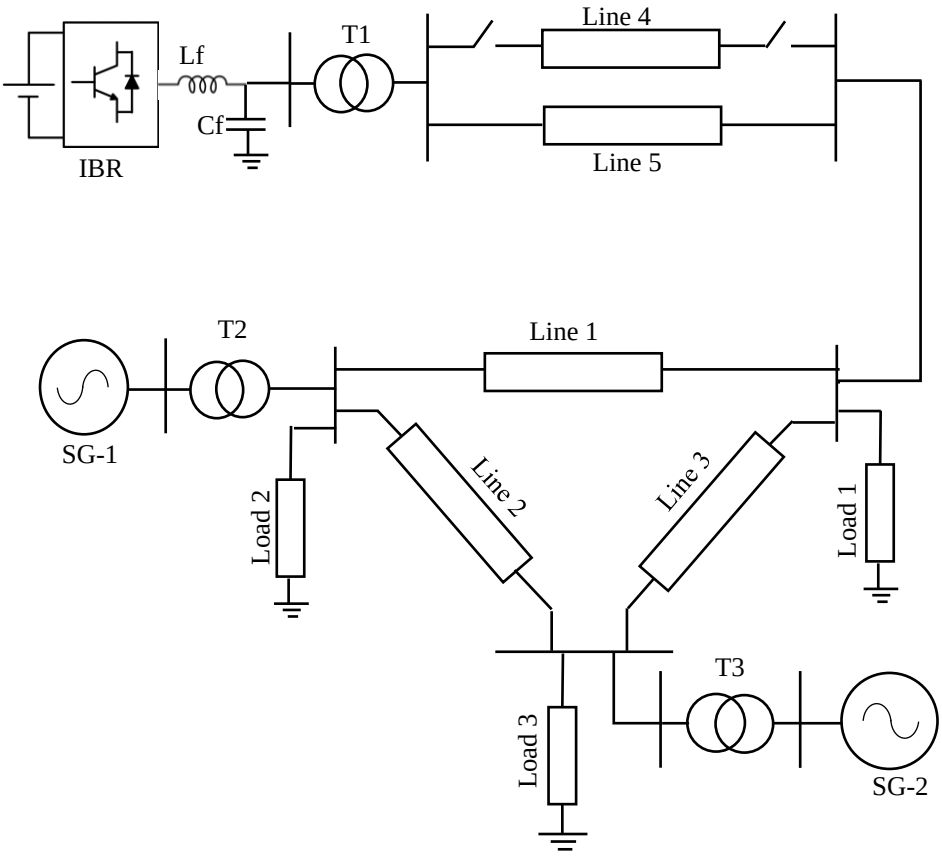

Figure 1.27 Schematic of the simulated multi-machine power system including an IBR

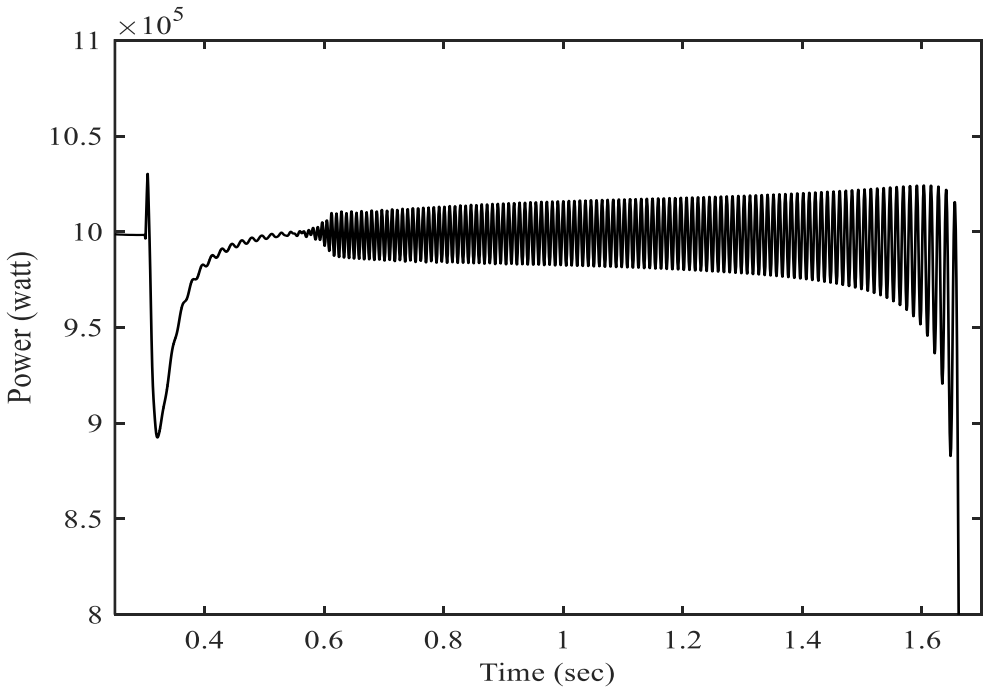

Figure 1.28 Output power of IBR, showing loss of grid synchronization

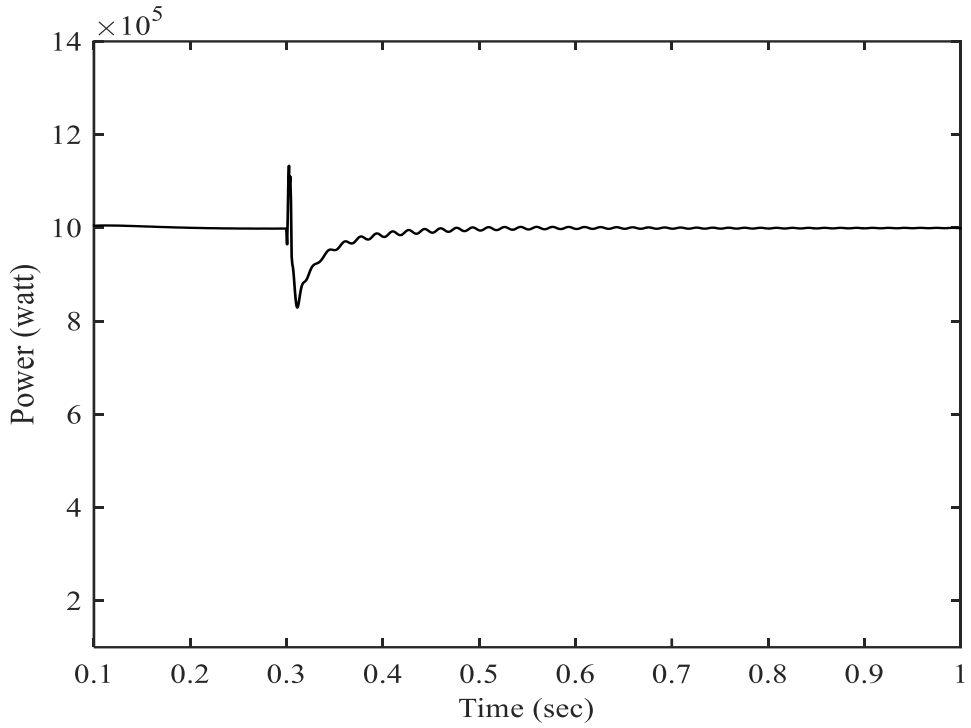

Figure 1.29 Output power of IBR, showing IBR retain its synchronization with the grid by slowing the PLL dynamic response.

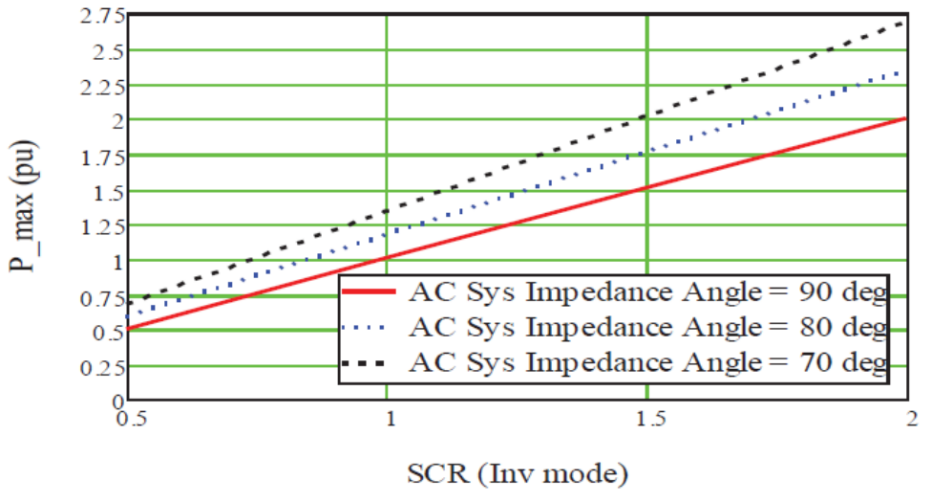

Figure 1.30 Inverter P_max vs SCR for different impedance angles [14]

1.7 Supplementary controller for enhancing inverters grid synchronization stability

According to Cigré Working Group B4.62 a connection is considered to be very weak if SCR at the Point of Interconnection (POI) is less than 3 in which SCR is defined as follows:

$$SCR = \frac{S_{SC}}{S_{Inverter}} = \frac{V_t^2}{|Z_s|S_{Inverter}} \tag{1.54}$$

Figure 1.30 [14] show the static transfer capacity limit as a function of SCR in which

$$P_{max}(P.U.) \approx SCR \cdot (1 + \frac{R_s}{|Z_s|}) \tag{1.55}$$

If dynamic stability limit is considered the situation is even worsened. It has been reported in [15] in some very weak systems SCR=1, only 40% of the maximum capacity of VSC can be used, even by turning the controllers parameters this limit can only reach to 60%. Therefore, proposing methods to enhance the grid synchronization stability of inverters is of special interest. Specifically, as discussed in the previous section, subsequent to the occurrence of events in power grids, depending on the post-event conditions of the system voltage, power and frequency oscillations may be experienced at the terminal of IBRs. If the strength of the system reduces, such oscillations are even further amplified and in extreme cases may lead to the disconnection of IBRs. While the existing controllers of IBRs have desirable tracking performances, their dynamic responses should be enhanced to overcome the above explained challenges in facing large disturbances in the power grid.

A supplementary controller is developed to overcome the above-mentioned shortcomings of existing controllers without replacing them. Figure 1.31, and 1.32 show the structure of the supplementary controller. The controller is designed based on the perturbed model of the control system. Washout filters are used to extract the perturbed components of the signals. In this way, it is possible to focus on high frequency components of the signals to damp out the high frequency

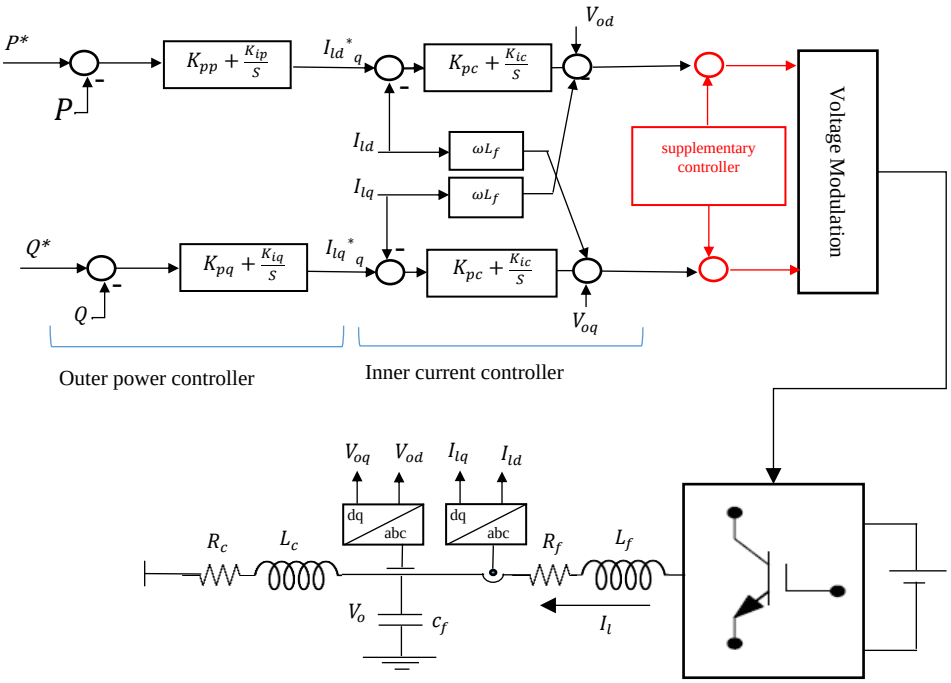

Figure 1.31 Schematic of the supplementary controller

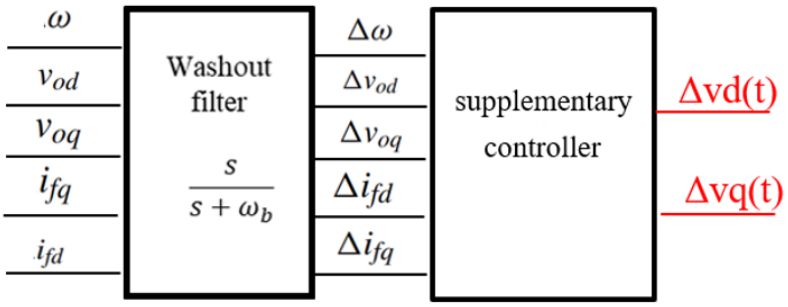

Figure 1.32 Schematic of the supplementary controller input and output signals

components. The advantage of the supplementary controller is it does not affect the tracking response of the main controller while it improves the transient response of the main controller. The perturbed model of IBRs in synchronous reference frame (SRF) should be derive as follow:

According to Figure 1.31, the state space model of synchronous reference frame (SRF) PLL is as follows:

$$\dot{\omega} = k_{P-PLL}(-\omega v_{od} + \frac{i_{fq}}{C_f} - \frac{i_{oq}}{C_f}) + k_{i-PLL} v_{oq}. \quad (1.56)$$

And also the dynamic of the output filter of the inverter is as follows:

$$C_f \dot{v}_{od} = C_f \omega v_{oq} + i_{fd} - i_{od} \quad (1.57)$$

$$C_f \dot{v}_{oq} = -C_f \omega v_{od} + i_{fq} - i_{oq} \quad (1.58)$$

$$L_f \dot{i}_{fd} = L_f \omega i_{fq} - v_{od} + v_{id} \quad (1.59)$$

$$L_f \dot{i}_{fq} = -L_f \omega i_{fd} - v_{oq} + v_{iq} \quad (1.60)$$

The state values are decomposed into the low frequency component and the high frequency component. Therefore, it is assumed $\omega = \omega_0 + \Delta\omega, v_{od} = V_{od} + \Delta v_{od}$, $v_{oq} = V_{oq} + \Delta v_{oq}$, $i_{oq} = I_{oq} + \Delta i_{oq}$ and $i_{fq} = I_{fq} + \Delta i_{fq}$ where ω_0 is the low frequency component of the angular frequency and $\Delta\omega$ is the high frequency component of the angular frequency. Replacing the above values in (1.56)-(1.60), the dynamic of perturbed model becomes as follows

$$\Delta\dot{\omega} = -k'_{P-PLL} C_f V_{od} \Delta\omega + k'_{P-PLL} \Delta i_{fq} + \Delta d_1. \quad (1.61)$$

Where

$$\Delta d_1 = k'_{P-PLL}\left[-C_f\Delta\omega\Delta v_{od} - C_f\omega_0\Delta v_{0d} - C_f\omega_0 V_{od} + I_{fd} - \left(I_{oq} + \Delta i_{oq}\right)\right] + k_{i-PLL}(V_{oq} + \Delta v_{oq}) - \dot{\omega}_0 \quad (1.62)$$

Similarly

$$C_f\Delta\dot{v}_{od} = C_f\Delta\omega\Delta v_{oq} + \Delta i_{fd} + \Delta d_2 \quad (1.63)$$

$$C_f\Delta\dot{v}_{oq} = -C_f\Delta\omega\Delta v_{od} + \Delta i_{fq} + \Delta d_3 \quad (1.64)$$

where $\Delta d_2, \Delta d_3$ are known inputs associated with the voltage dynamics and are derived as follows:

$$\Delta d_2 = C_f V_{oq}\Delta\omega + C_f\omega_0\Delta v_{0q} + C_f\omega_0 V_{oq} - (I_{od} + \Delta i_{od}) + I_{fd} - C_f\dot{V}_{od} \quad (1.65)$$

$$\Delta d_3 = -C_f V_{od}\Delta\omega - C_f\omega_0\Delta v_{0d} - C_f\omega_0 V_{od} - (\Delta i_{oq} + I_{oq}) + I_{fq} - C_f\dot{V}_{oq} \quad (1.66)$$

Similarly

$$L_f\dot{\Delta i}_{fd} = L_f\Delta\omega\Delta i_{fq} - \Delta v_{od} + \Delta v_{id} + \Delta d_4 \quad (1.67)$$

$$L_f\dot{\Delta i}_{fq} = -L_f\Delta\omega\Delta i_{fd} - \Delta v_{oq} + \Delta v_{iq} + \Delta d_5 \quad (1.68)$$

Where Δd_4 and Δd_5 are expressed as follows:

$$\Delta d_4 = L_f\Delta\omega I_{fq} + L_f\omega_0\Delta i_{fq} + L_f\omega_0 I_{fq} - V_{od} + v_{id}^{ref} - L_f\dot{I}_{fd} \quad (1.69)$$

$$\Delta d_5 = -L_f\Delta\omega I_{fd} - L_f\omega_0\Delta i_{fd} - L_f\omega_0 I_{fd} - V_{oq} + v_{iq}^{ref} - L_f\dot{I}_{fq} \quad (1.70)$$

Where L_f and C_f are inductance and capacitance of output filter, Δi_{od}, Δ_{ioq} are direct/quadratic perturbed components of output current, I_{fd},I_{fq},I_{od},I_{oq} are DC components of direct/quadratic currents, Δi_{fd}, Δi_{fq} direct/quadratic perturbed components of current at the output filter of the inverter, V_{od}, V_{oq} are DC components of direct/quadratic voltages, Δv_{od}, Δv_{oq} direct/quadratic perturbed components of voltage at output capacitor, K_{P-PLL}, k_{i-PLL} proportional and integral gains for PLL, ω, ω_C, ω_n, ω_0, $\Delta\omega$, Angular frequency, DC components of angular frequency, angular frequency perturbation, the cut-off frequency of the filter and nominal angular frequency

Equations (1.61), (1.63), (1.64), (1.67) and (1.68) constitute the perturbed state space model of the IBR. To derive the perturbed term, a set of wash-out filters are used. According to the perturbed model of IBR, we are developing controllers to attenuate the disturbances (i.e. perturbed terms), which is the ongoing task.

Once the state space model of the perturbed system is developed, a variety of controllers can be designed. Specifically, in [1] we developed a supplementary controller based on the

interconnection damping assignment passivity based (IDA-PB) control strategy. The controller is applied to the IBR in Figure 1.27. At t=5 the strength of the system is reduced by taking the line out. Figure 1.33-(a) shows output of the inverter. As Figure 1.33-(b) shows the supplementary controller successfully damped out the oscillations and prevented instability.

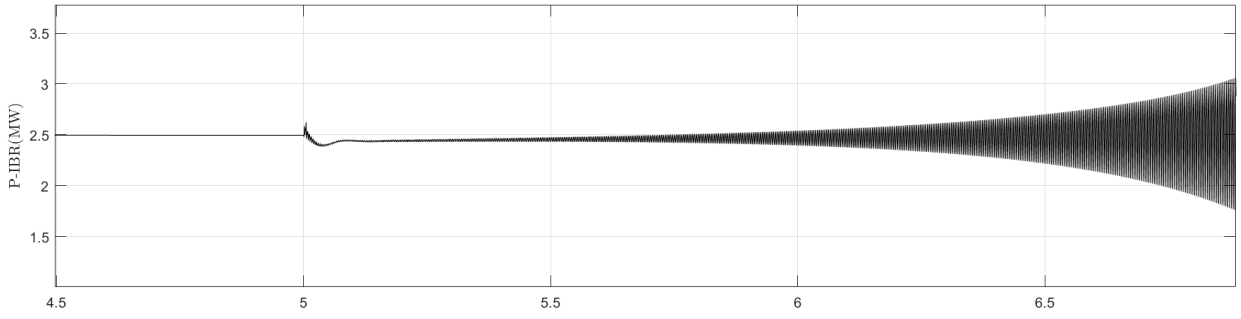

(a)

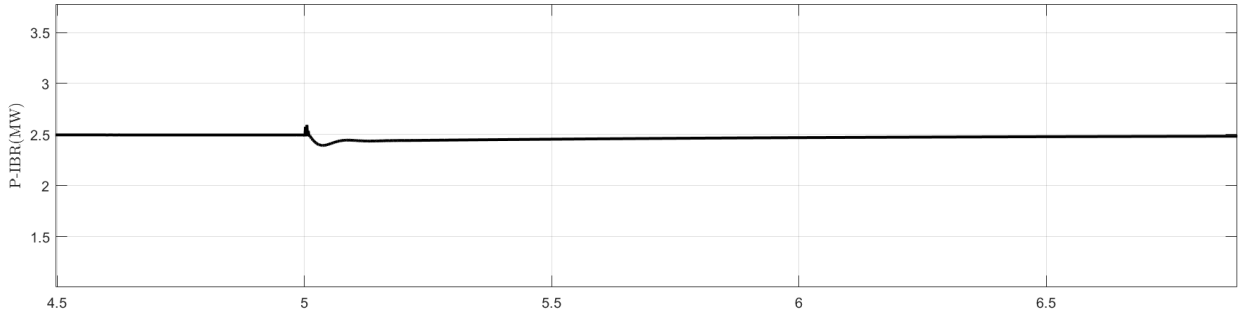

(b)

Figure 1.33 Output power of inverter (a) without the supplementary controller (b) with the supplementary controller

1.8 Conclusions

In this project the grid synchronization stability of inverter-based resources was studied. Using Bode plots and Generalized Nyquist Criterions (GNC) the impacts of different parameters such as the synchronization mechanism via PLL and grid strength were studied. The case studies results showed in weak power grids the bandwidth of PLL is influential on the grid synchronization stability. To accurately study the impact of grid strength GNC was utilized, and off-diagonal elements were not ignored. This is crucial for correct assessment of the grid synchronization stability. The simulation results demonstrated by making the PLL slower the grid synchronization stability can be improved but a slow PLL can not track fast changing of the system. To address this problem a supplementary controller was implemented based on perturbed model of the system. It adds damping to the system to damp out the output power oscillations leading to enhanced synchronization stability. It does not change the main controllers of the inverters and only adds supplementary signals to the controller which becomes zero at the steady state condition. Therefore, the supplementary controller improves the transient response of the controller which does not affect its proper tracking characteristics.

References

[1] M. Azimi, S. Lotfifard, ”Supplementary Controller for Inverter-based Resources in Weak Power Grids” IEEE Transactions on Smart Grid, vol.13, no.4, pp. 2886-2896, 2022.

[2] J. Schmall, S. Huang, Y. Li, J. Billo, J. Conto, Y. Zhang, “Voltage Stability of Large-Scale Wind Plants Integrated in Weak Networks: An ERCOT Case Study” IEEE PES General Meeting, pp.1-5, 2015.

[3] P.C. Kjaer, M. Gupta, A. Martinez, S. Saylors, “Experiences with Wind Power Plants with Low SCR” IEEE PES General Meeting, 2015.

[4] L. Petersen, B. Hesselbæk, A. Martinez, R. M. Borsotti-Andruszkiewicz, G. C. Tarnowski, N. Steggel, D. Osmond, “Vestas Power Plant Solutions Integrating Wind, Solar PV and Energy Storage”. 3rd International Hybrid Power Systems Workshop, 2018.

[5] T. Ackermann “Wind Power in Power Systems” Wiley, 2005.

[6] M. Morjaria “Deploying Utility-Scale PV Power Plants in Weak Grids” PES general meeting, 2017.

[7] R. Musca, G. Zizzo, M. Bongiorno “Grid-Forming Converters in Weak Grids – The Case of a Mediterranean Island” 18th International Workshop on Large-Scale Integration of Wind Power into Power Systems as well as on Transmission Networks for Offshore Wind Power Plants, pp. 1-6, 2019.

[8] S. Liemann, T. Hennig, L. Robitzky, C. Rehtanz, and M. Finkelmann,“Analysis of the stability and dynamic responses of converter-based gener-ation in case of system splits,”IET Gener., Transmiss. Distribution, vol. 13,no. 16, pp. 3696–3703, 20 8 2019.

[9] A. Yazdani, R. Iravani,”Voltage-Sourced Converters in Power Systems: Modeling, Control, and Applications” Wiley-IEEE Press, 2010.

[10] B. wen, D. Boroyevich, R. Burgos, P. Mattavelli and Z. Shen, "Analysis of DQ small-signal impedance of grid-tied inverters," IEEE Transactions on Power Electronics, vol. 31, no. 1, pp. 675-687, 2015.

[11] J. Yu, X. Lin, D. Song, R. Yu, Y. Li, and M. Su “Harmonic Instability and Amplification for Grid-Connected Inverter With Voltage Harmonics Compensation Considering Phase-Locked Loop” IEEE Journal of Emerging and Selected Topics in Power Electronics, vol. 8, no 4, 2020.

[12] C. Desoer and Y. T. Wang, "On the generalized Nyquist stability criterion," IEEE Transactions on Automatic Control, vol. 25, no. 2, pp. 187-196, 1980.

[13] M. Cheah-Mane, A. Egea-Alvarez, E. Prieto-Araujo, H. Mehrjerdi, O. Gomis-Bellmunt, L. Xu, “Modeling and analysis approaches for small-signal stability assessment of power-electronic-dominated systems” Wiley Interdisciplinary Reviews: Energy and Environment, pp. 1-22, 2023.

[14] J. Z. Zhou, and A. M. Gole VSC “Transmission limitations imposed by AC system strength and AC impedance characteristics” 10th IET International Conference on AC and DC Power Transmission, 2012.

[15] M. Ashabani and Y. Abdel-Rady I. Mohamed, “Integrating VSCs to Weak Grids by Nonlinear Power Damping Controller With Self-Synchronization Capability” IEEE Transactions on Power Systems, vol. 29, no. 2, 805-814, 2014.